Distortion Immunity of MLS-Derived Impulse Response Measurements

Chris Dunn and Malcolm Hawksford

Audio Research Group, Department of Electronic Systems Engineering
University of Essex

email: chris.dunn@scalatech.co.uk

Maximum length sequence (MLS) measurement of system impulse responses offers a potential enhancement in error immunity over periodic impulse testing, although care must be exercised in setting the MLS excitation amplitude in order to realise this potential. The effects of nonlinearity in MLS measurement are studied, in particular the way in which impulse response errors due to nonlinearity are distributed across the measurement period. The consequences of such errors in cumulative spectral display plots are also investigated. Finally inverse-repeat sequences (IRS) are shown to have complete immunity to even-order nonlinearity while maintaining many of the advantages of MLS.

0 INTRODUCTION

Perhaps the most fundamental evaluation of an audio system is the determination of the linear transfer function, defined by the impulse response (IR) in the time domain from which the frequency response can be calculated. Some applications require highly accurate linear transfer function measurement, for example equalisation of loudspeakers in the digital domain where measurement accuracy must match equalisation performance (*i.e.* better than ± 0.5 dB across wide regions of the audio spectrum - see for example [1]). Another application that requires highly accurate linear transfer function measurement is a technique proposed by the authors to measure low level errors within audio systems [2].

There are three established methods of linear transfer function measurement - periodic impulse excitation (PIE), maximum length sequences (MLS), and time delay spectrometry (TDS). PIE reveals the periodic impulse response (PIR) of the device under test (DUT) directly by applying a periodic short duration impulse to the DUT and measuring the output [3]. The main problem encountered in PIE is poor noise immunity due to low excitation signal energy; this drawback can be overcome to some degree by averaging several measurements. Alternatively an MLS can be used, which, compared to a periodic impulse of similar repetition rate, has a much higher excitation energy for the same peak output (*i.e.* a lower crest factor). An MLS is a pseudo-random binary sequence which yields a unit impulse upon circular autocorrelation and this property allows the PIR of a test system to be obtained by applying an MLS to the DUT and cross-correlating the system output with the input. An excellent introduction to MLS techniques is provided by Rife and Vanderkooy [4]. PIE and MLS initially reveal the transfer function in the time domain while TDS methods yield transfer function information as a complex frequency response (which can of course be converted to the time-domain by using the inverse Fourier transform). TDS techniques utilise swept sine waves or "chirps" which are input to the DUT and recover the complex frequency response of the test system after hardware or software processing [5]. Both TDS and MLS offer an increase in noise and distortion immunity over PIE. However, it can be shown that in achieving a similar frequency resolution to that available from MLS, a typical TDS implementation will take considerably longer to execute [4], [5], [6]. The additional disadvantage that TDS suffers in terms of hardware and software complexity [7] also helps to explain the growing popularity of MLS [8], [9].

Noise and distortion present in any practical measurement environment reduces the accuracy of linear transfer function measurement. A simulated example of the effects that nonlinearity can have upon impulse measurement is shown in Fig. 1. The true magnitude response in the frequency-domain [Fig. 1(a)] of a 1 kHz lowpass FIR filter with less than 0.001 dB pass-band ripple can be compared against the

MLS-derived magnitude response of the same filter in Fig. 1(b), where the measurement has been corrupted by gross second-order nonlinearity. Clearly the distortion has caused the recovered transfer function to appear much more ragged over the filter's pass-band than its linear specification would suggest.

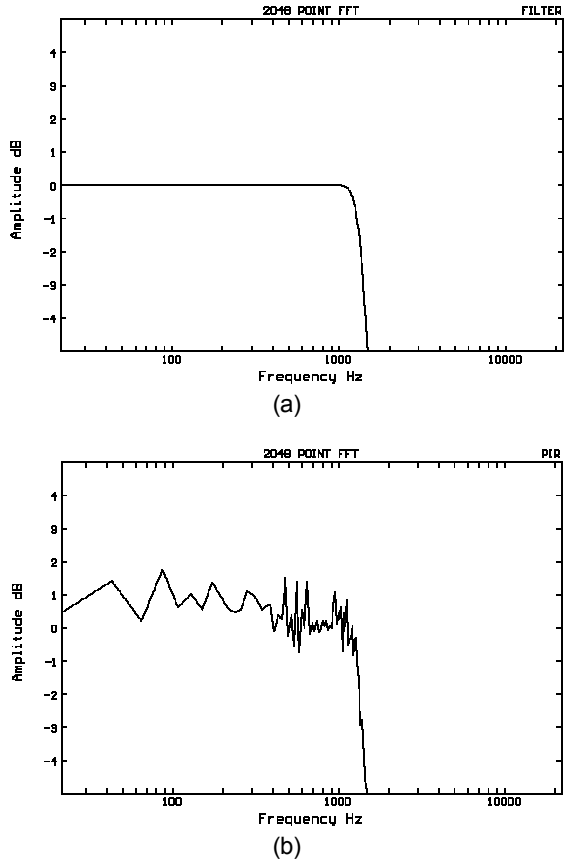

Fig. 1. (a) Magnitude response of 1 kHz lowpass FIR filter. (b) MLS-derived magnitude response of same filter where measurement has been corrupted by gross second-order nonlinearity.

This paper investigates by simulation the effects that nonlinearity can have upon MLS measurement. In particular we examine the way in which errors due to nonlinearity are spread across the period of the recovered impulse response, and the consequences of such distributions for increasing distortion immunity by truncating the impulse response. A comparison of overall (noise *and* distortion) error immunity between MLS and PIE techniques is followed by an assessment of the suitability of inverse repeat sequences (IRS) for linear transfer function measurement.

1 DETERMINING DISTORTION IMMUNITY BY SIMULATION

Any system with weak (i.e. non-overloading) nonlinearity can be modelled in the frequency domain by the nonlinear transfer function shown in Fig. 2(a) [4]. This includes a linear stage $H(f)$ and nonlinear stages $H(f_1, f_2)$, $H(f_1, f_2, f_3)$ etc., which represent different distortion orders. When a multitone signal is input to the model, harmonic and intermodulation error products will corrupt the output signal. Nonlinearity can also be represented in the time-domain as a distributed model [Fig. 2(b)], where distortion polynomials d_m appear in parallel with linear filters h_m. Although the distributed time-domain model is capable of modelling complex nonlinearities, we require a simpler model for simulation. The nonlinear model used throughout

this paper is similar to that used by Rife and Vanderkooy in a previous study of distortion in MLS measurements [4], consisting of a filter $h(n)$ followed by a nonlinearity $d\{\ \}$ [Fig. 2(c)]. For most of the simulations presented in this paper the nonlinearity is memoryless, *i.e.* the error sequence output from the nonlinear stage depends solely upon its instantaneous input, and the characteristics of the nonlinearity are thus independent of frequency. Despite the simplicity of this model, it is a fairly good representation of many physical nonlinear processes. For example a signal applied to a loudspeaker will typically pass through a crossover filter circuit before reaching the drive unit, which itself will tend to limit at its `output' as excursion limits are approached. Furthermore a practical MLS measurement system will employ some lowpass filtering before the MLS is applied to the DUT in order to minimise slew-related artifacts in the recovered impulse response [10], [11]. In fact, prefiltering the MLS or PIE excitation is a necessary condition that must be met if the nonlinearity is to change the shape of the recovered impulse response. If unfiltered MLS or PIE signals are input to a memoryless nonlinearity then the binary excitation will merely result in a DC offset error in the recovered impulse response for even-order nonlinearity or a pure gain change error for odd-order nonlinearity.

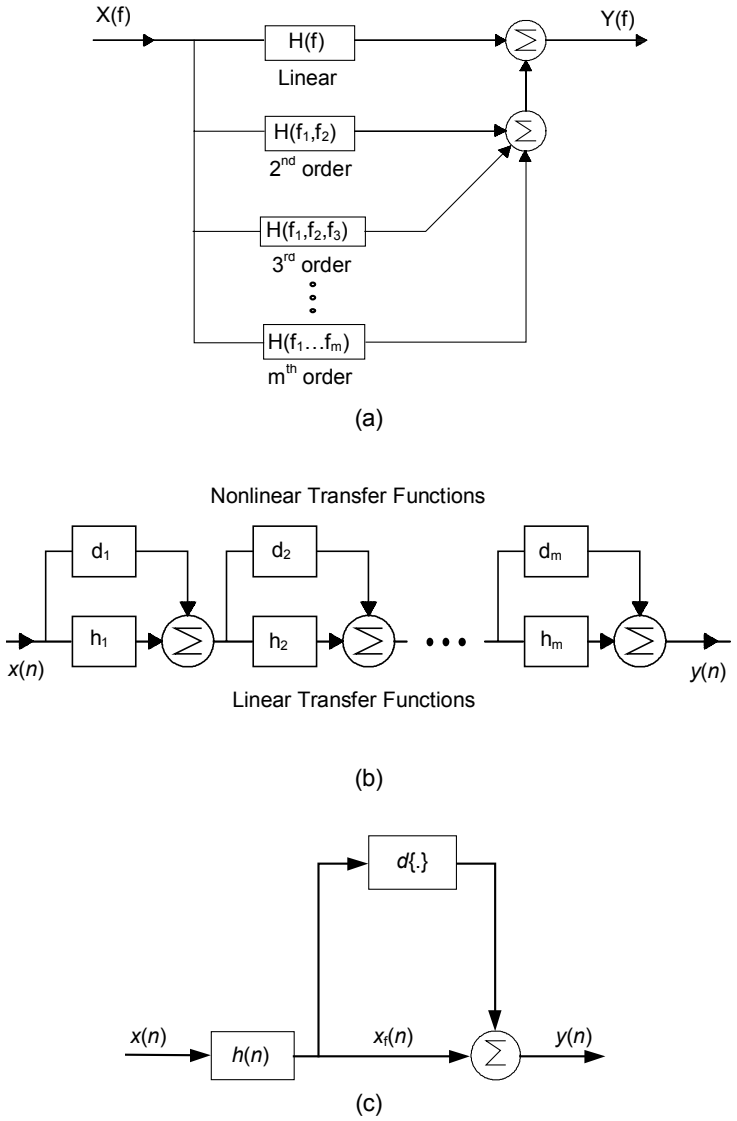

Fig. 2. Nonlinear system modelling. (a) Frequency-domain model. (b) Distributed time-domain model. (c) Lumped time-domain model.

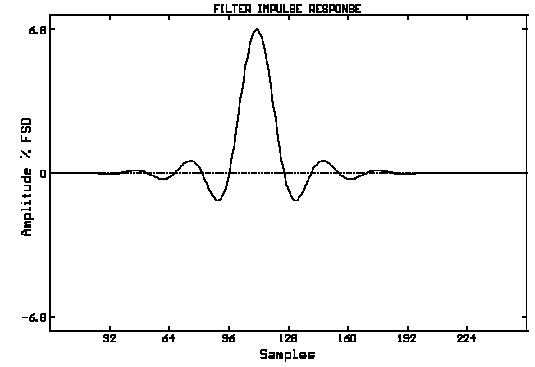

(a)

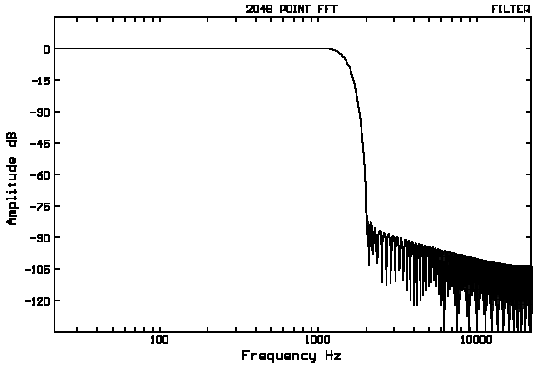

(b)

Fig. 3. 1 kHz FIR lowpass filter. (a) Time-domain impulse response $h(n)$. (b) Frequency-domain magnitude response.

We will now describe the general simulation process used to determine distortion immunity in impulse response measurements. A periodic driving signal $x(n)$ (either a PIE or an MLS) is convolved with a known linear impulse response $h(n)$ over a measurement period L of 2047 samples. Unless otherwise indicated, $h(n)$ is a 1 kHz lowpass FIR filter, the first 256 samples of which are plotted in the time domain in Fig. 3(a). Noting that the sampling frequency is set to 44.1 kHz, the frequency-domain magnitude response of the filter is illustrated in Fig. 3(b). If $h(n)$ is non zero for a time less than the period of the driving signal, then time aliasing in the convolution operation is avoided and just one period is required in the simulations to accurately describe the periodic system behaviour. The filtered driving signal $x_f(n)$ is distorted by a known polynomial $d\{\ \}$, and after appropriate postprocessing has extracted the distorted impulse response $h_o(n)$, the error component $e(n)$ can be calculated by subtracting the known $h(n)$ from $h_o(n)$. The simulation process therefore allows us to examine the impulse error sequence $e(n)$ associated with a particular nonlinearity $d\{\ \}$. Summarising the general simulation procedure,

$$\begin{aligned} x_f(n) &= x(n) \otimes h(n) \\ y(n) &= x_f(n) + d\{x_f(n)\} \\ h_o(n) &= P[y(n)] \\ e(n) &= h_o(n) - h(n) \end{aligned} \tag{1}$$

where $\otimes$ represents convolution;
$y(n)$ is the distorted output driving signal;
$P[\ ]$ represents the post-processing operation required to yield an impulse response from the output driving signal.

In general a memoryless r^{th}-order nonlinearity $d\{\ \}$ can be written:

$$d\{x_f(n)\} = A_d\left[\frac{x_f(n)}{x_{ref}}\right]^r \tag{2}$$

where A_d sets the amplitude of the nonlinearity and x_{ref} is a reference scaling level. We must set x_{ref} such that a valid comparison can be made between PIE and MLS error immunity. The obvious choice is to adopt an "absolute scaling" where $x_{ref} = 1$, and make the peak levels of the unfiltered PIE and MLS signals equal (so that the noise immunity advantage of MLS is known [4]). Thus a third-order nonlinearity at -20 dB would be written

$$d\{x_f(n)\} = 0.1[\,x_f(n)\,]^3 \quad . \tag{3}$$

All of the variables used in the simulations are represented by double-precision floating-point numbers which offer a relative error due to mantissa quantisation of 2^{-53} (-319 dB).

2 PIE DISTORTION IMMUNITY

Periodic impulse testing reveals the periodic impulse response of the system under investigation directly by applying a periodic impulse to the DUT and sampling the output signal. Physically this excitation can be obtained using a pulse generator or one of the many test compact discs with a periodic impulse signal track. No postprocessing upon the measured system output signal is required (although averaging several impulse periods can improve random noise immunity - see Sec. 4), and the PIE simulation process can be summarised as:

$$\begin{aligned} x(n) &= \delta(n) \\ x_f(n) &= h(n) \\ P[y(n)] &= y(n) \\ e(n) &= d\{x_f(n)\} \quad . \end{aligned} \tag{4}$$

Referring to Eq. (2), we now examine the consequences of second-order nonlinearity by setting $r = 2$ and the distortion level $A_d = 0.1$ (-20 dB). The first 256 samples of the error sequence $e(n)$ is plotted in the time-domain in Fig. 4(a), and can be seen to contain a large peak coincident with the linear impulse response (the amplitude scaling in the time-domain plots is relative to the peak level of the unfiltered driving signal). In general the error due to nonlinearity will contain a `linear' component $e_l(n)$ identical in shape to the linear impulse response of the system, and also a nonlinear part $e_{nl}(n)$. It is the nonlinear component $e_{nl}(n)$ of the impulse error which causes the raggedness seen in the magnitude response of the example presented in Fig. 1. Conversely the linear component $e_l(n)$ represents a gain change in the measurement, *i.e.* the observed gain of the system under examination has changed due to nonlinearity. With some applications this gain change is important, see for example [2], but in many situations such as loudspeaker testing we are interested in the *relative* linear transfer function rather than the absolute gain of the DUT. Hence in our study of distortion immunity it is useful to be able to distinguish between linear and nonlinear errors in the impulse response measurement. We can perform such an `error normalisation' by subtracting a scaled version of the linear impulse response $h(n)$ from the overall error sequence $e(n)$,

$$e_{nl}(n) = e(n) - g\,h(n). \tag{5}$$

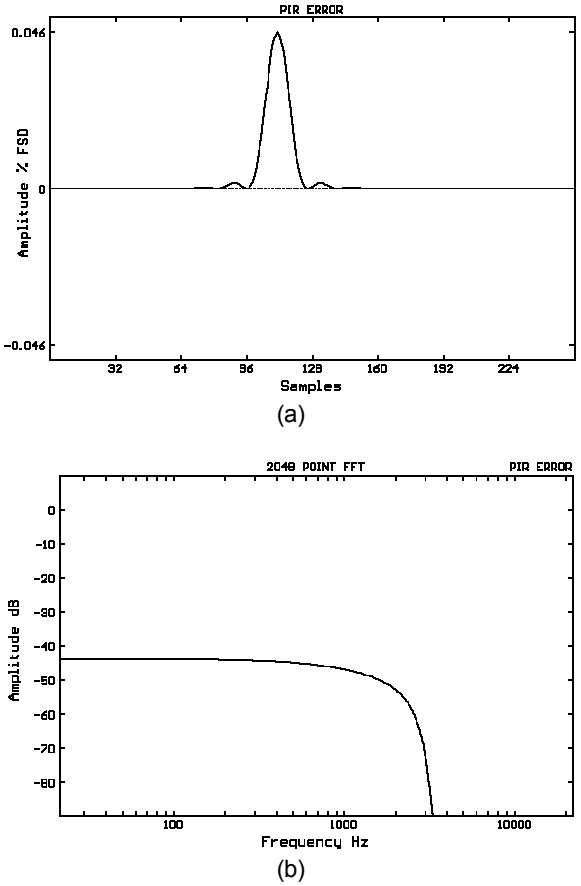

Fig. 4. PIE-derived error due to second-order nonlinearity.
(a) Time domain $e(n)$. (b) Frequency domain.

It is easy to show that $e_{nl}(n)$ is minimised in an rms sense by setting the gain error g to

$$g = \frac{\sum_{k=0}^{L-1} e(k)\,h(k)}{\sum_{k=0}^{L-1} h(k)^2} \quad . \tag{6}$$

This analysis of gain change due to nonlinearity is similar to the study undertaken by Vanderkooy [11]. Fig. 5 shows the nonlinear component of the overall error shown in Fig.4.

The distortion immunity I_d of the impulse measurement is calculated as the ratio of linear impulse response energy to nonlinear error energy:

$$I_d = 10 \log_{10} \left[\frac{\sum_{k=0}^{L-1} h(k)^2}{\sum_{k=0}^{L-1} e_{nl}(k)^2} \right] \quad . \tag{7}$$

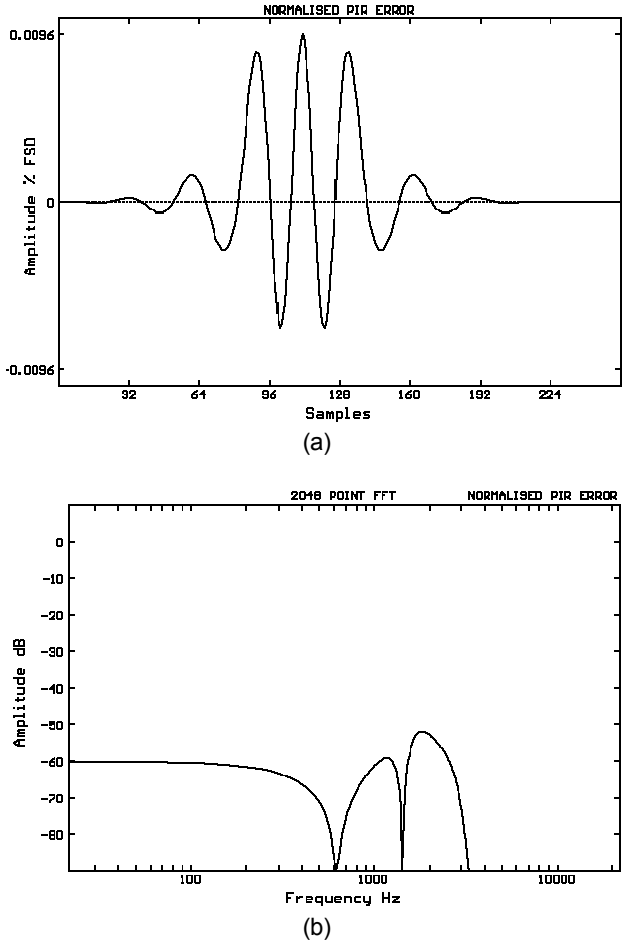

Fig. 5. PIE-derived normalised nonlinear error due to second-order nonlinearity. (a) Time domain $e_{nl}(n)$. (b) Frequency domain.

Simulations were performed for second- to seventh-order nonlinearity with the 1 kHz lowpass FIR filter and distortion immunity tabulated in Table 1. The accuracy of the PIE simulations is extremely high because:

(i) the error sequence can be calculated directly [Eq. (4)], rather than by subtracting the $h_o(n)$ sequence from $h(n)$ as described in Sec. 1 [Eq. (1)], and

(ii) no postprocessing operation is required.

Direct calculation of $e_{nl}(n)$ allows simulated distortion immunity to exceed the limits that would otherwise be present due to mantissa quantisation in the floating-point variables. Theoretically, the *maximum* distortion immunity that can be recorded using this simulation technique is bounded by the *range* of the simulation variables - which is of the order of 6000 dB for double-precision floating-point numbers. The PIE distortion immunity results collated in Table 1 are well below this limit. The *relative error* of $e_{nl}(n)$ (*i.e.* the error of the impulse error sequence) *is* limited by quantisation effects in the floating point variables at approximately -300 dB.

Table 1. Distortion immunity of impulse response measurements for 1 kHz FIR lowpass filter with A_d = -20 dB.

Distortion Order	PIE Distortion Immunity dB	MLS Distortion Immunity dB	IRS Distortion Immunity dB
2	54.7	29.4	> 262
3	77.2	35.4	36.6
4	99.7	35.9	> 265
5	123	38.4	41.4
6	146	39.7	> 267
7	169	41.4	46.2

Table 2. Noise immunity advantage of MLS over PIE for 1 kHz FIR lowpass filter, when distortion immunity has been normalised. Results extrapolated from Table 1 data and confirmed by additional simulations.

Distortion Order	Distortion Immunity dB	Relative MLS Excitation Amplitude dB	MLS Noise Immunity Advantage dB
2	54.7	-25.3	7.8
3	77.2	-20.9	12.2
4	99.7	-21.3	11.8
5	123	-21.2	11.9
6	146	-21.3	11.8
7	169	-21.3	11.8

Table 3. Distortion immunity of impulse response measurements for 10 kHz FIR lowpass filter with A_d = -20 dB.

Distortion Order	PIE Distortion Immunity dB	MLS Distortion Immunity dB	IRS Distortion Immunity dB
2	36.4	21.9	> 263
3	42.4	23.9	23.9
4	47.6	16.6	> 254
5	53.3	16.1	16.1
6	59.2	10.6	> 246
7	65.3	8.9	8.9

Table 4. Noise immunity advantage of MLS over PIE for 10 kHz FIR lowpass filter, when distortion immunity has been normalised. Results extrapolated from Table 3 data and confirmed by additional simulations.

Distortion Order	Distortion Immunity dB	Relative MLS Excitation Amplitude dB	MLS Noise Immunity Advantage dB
2	36.4	-14.5	18.6
3	42.4	-9.3	23.8
4	47.6	-10.3	22.8
5	53.3	-9.3	23.8
6	59.2	-9.7	23.4
7	65.3	-9.4	23.7

3 MLS DISTORTION IMMUNITY

3.1 Review of MLS Measurement Techniques

Maximum length sequences are pseudorandom binary signals that can be generated from digital shift registers with appropriate EXCLUSIVE-OR feedback structures. If an MLS $s(n)$ is generated from an mth-order shift register (*i.e.* one with m stages), then all shift register states bar one (all 0's) are included in each MLS period of length L. Thus $L = 2^m-1$ samples. Fig. 6(a) shows a fifth-order MLS where the (1,0) shift register logic output has been transformed to (-1,1) scaled voltages and a zero-order hold is used between samples. If we follow the convention adopted by Rife and Vanderkooy [4] of scaling autocorrelation and cross-correlation operations by $1/(L+1)$ rather than the usual $1/L$, then the first-order circular autocorrelation Ω_1 of an MLS is a unit impulse with a DC offset:

$$\begin{aligned} \Omega_1(n) &= s(n) \Phi s(n) \\ &= \frac{1}{L+1} \sum_{k=0}^{L-1} s(k)s(k+n) \\ &= \delta(n) - \frac{1}{L+1}, \qquad 0 \le n < L. \end{aligned} \tag{8}$$

where Φ represents circular cross-correlation and all indices within the summation are calculated mod L. Fig. 6(b) shows the autocorrelation of the fifth-order sequence shown in Fig. 6(a). When an unfiltered MLS is applied to a linear system with impulse response $h(n)$ of length less than the period of the MLS, then cross-correlating the input and output of the system recovers the AC component of $h(n)$ together with an attenuated DC component [4]:

$$
\begin{aligned}
s(n)\,\Phi\, y(n) &= \frac{1}{L+1}\sum_{k=0}^{L-1} s(k)\,y(k+n) \\
&= \left[h(n) - \frac{1}{L}\sum_{k=0}^{L-1} h(k)\right] + \left[\frac{1}{L(L+1)}\sum_{k=0}^{L-1} h(k)\right] \qquad (9) \\
&= h_{AC}(n) + \frac{1}{L+1}\,h_{DC}(n)\ .
\end{aligned}
$$

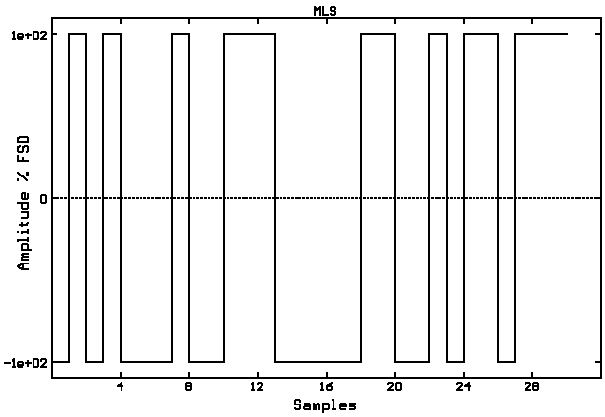

(a)

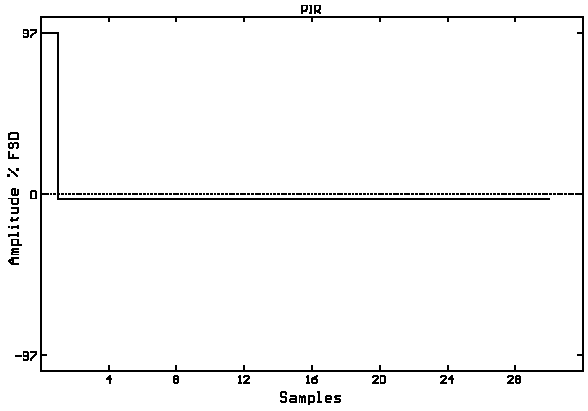

(b)

Fig. 6. (a) Unfiltered 31-point MLS $s(n)$ generated from fifth-order shift register with zero-order hold. (b) Autocorrelation $\Omega_1(n)$ of (a).

In many applications such as loudspeaker testing the DUT will be AC coupled, and so the DC component will essentially be equal to zero. A practical MLS measurement system based around a personal computer would generate the MLS excitation using a shift register either in software or hardware. The MLS is applied to the input of the DUT and the output signal sampled using an analog-to-digital converter (ADC) over at least one measurement period after the system has settled to steady state operation. The measured output sequence is then cross-correlated with the known input sequence to reveal the impulse response of the system. There are several methods of performing the cross-correlation, the most efficient of which is by fast Hadamard transform (FHT) where an L-point cross-correlation can be performed with only 2.5 $L \log_2 L$ floating point additions - see Borish and Angell [12] and Borish [13] for details.

3.2 MLS Distortion Immunity

We analyse MLS distortion immunity using an eleventh-order sequence with EXCLUSIVE-OR feedback taps from the second and eleventh shift register stages [13]. This results in a commonly used sequence period of 2047 samples. The MLS signal is convolved with the linear impulse response of the simulated system, again the 1 kHz lowpass FIR filter shown in Fig. 3. The MLS convolution, like an MLS cross-correlation, is most efficiently performed by FHT [14]. Distorting the convolved driving signal will corrupt the impulse response obtained from the measurement, but the nature of the distortion is different from that of a PIE-derived measurement because of the postprocessing cross-correlation operation:

$$\begin{aligned} P[y(n)] &= s(n) \Phi\, y(n) \\ &= \frac{1}{L+1} \sum_{k=0}^{L-1} s(k)\, y(n+k) \quad . \end{aligned} \tag{10}$$

The effect that nonlinear distortion has upon MLS-derived impulse responses is shown in Fig. 7. The 1 kHz FIR lowpass filter whose full impulse response $h(n)$ is shown in Fig. 7(a) is convolved with the 2047-point MLS, resulting in the filtered MLS signal in Fig. 7(b). The filtered MLS signal is then distorted by second-order nonlinearity, and the result cross-correlated with the unfiltered MLS to recover the corrupted impulse response $h_o(n)$ in Fig. 7(c). Although for most of the simulations in this paper we have adopted a distortion amplitude A_d = -20 dB, in this example we have set A_d = -10 dB in order to clearly show the nature of the artifacts in the recovered impulse response (the amplitude of the nonlinearity does not change the shape of the impulse error, just its amplitude relative to the linear impulse response). Immediately evident is the "spiky" or "lumpy" nature of the error in the tail of the impulse response, an observation which has been noted many times [10], [15], [16], [4], [17], [11].

Because cross-correlation is a distributive process, impulse error $e(n)$ can be calculated by cross-correlating $s(n)$ with the driving sequence distortion $d\{x_f(n)\}$. Again, this has the benefit of increasing simulation accuracy since calculating $e(n)$ does not now involve a subtraction from $h(n)$. The MLS simulation summary is thus:

$$\begin{aligned} x(n) &= s(n) \\ x_f(n) &= s(n) \otimes h(n) \\ e(n) &= s(n) \Phi\ d\{x_f(n)\} \ . \end{aligned} \tag{11}$$

The nonlinear component $e_{nl}(n)$ of $e(n)$ is calculated using the methodology described in Sec. 2. Although the error is calculated directly [Eq. (11)], the accuracy of the MLS simulations is not as high as that obtained from the PIE experiments. The cross-correlation postprocessing operation required for MLS involves $\log_2(L/2)$ floating-point additions or subtractions for each error sample when the fast Hadamard transform is used, hence the theoretical maximum MLS distortion immunity that can be recorded using this simulation technique is bounded by floating-point mantissa quantisation at approximately 300 dB. The results recorded in Tables 1 - 4 are well within this limit.

Fig. 8 shows the impulse distortion $e(n)$ due to a second-order nonlinearity for A_d = -20 dB. Because a filtered MLS possesses an approximately symmetrical amplitude distribution, then even-order nonlinearity results in very low gain error, and the normalised error sequence is very similar to the unnormalised error [11]. However, odd-order memoryless nonlinearity results in a large error sequence component that is co-incident with the linear impulse response, and error normalisation thus results in a significant fall in error level. For example, the third-order impulse error with the 1 kHz filter falls by 4 dB after normalisation (compare Figs. 9 and 10). Table 1 presents the simulation results for (untruncated) MLS distortion immunity with the 1 kHz filter and nonlinearities ranging from second- to seventh-order.

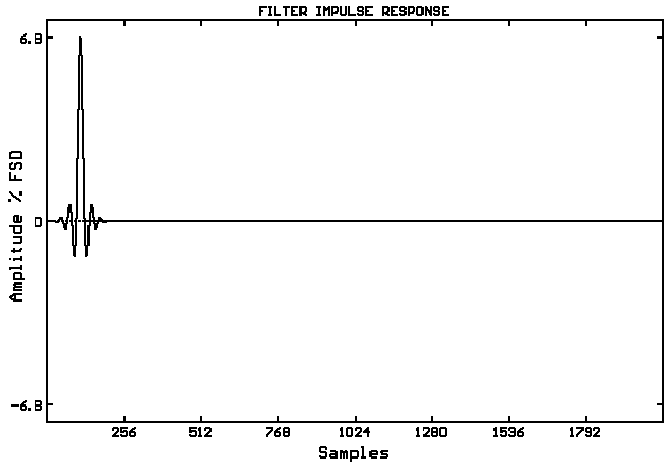

(a)

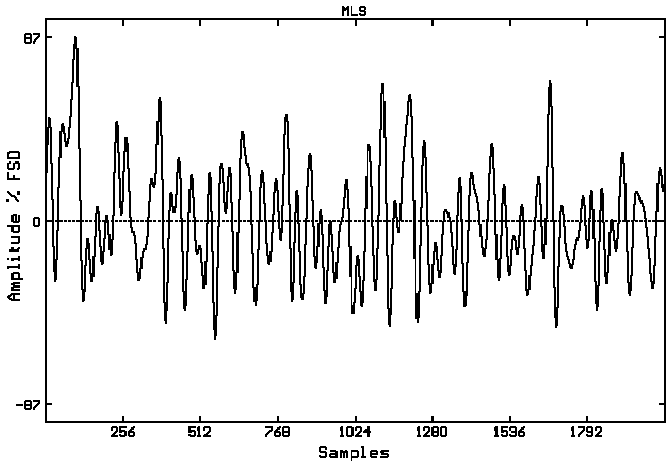

(b)

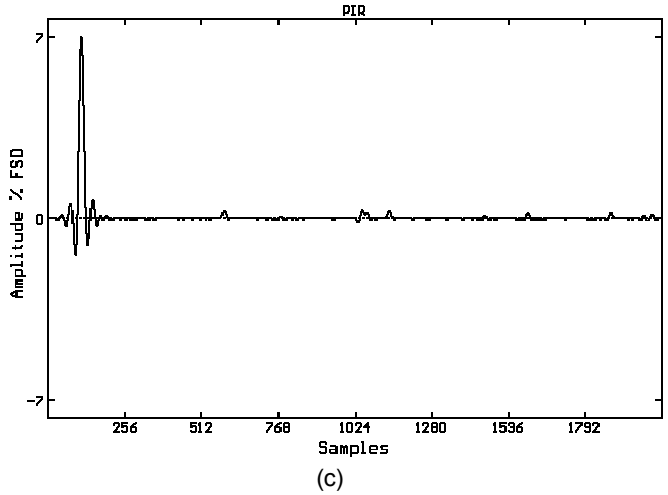

(c)

Fig. 7. (a) Impulse response $h(n)$ of 1 kHz lowpass FIR filter. (b) MLS signal after filtering with 1 kHz lowpass filter. (c) MLS-derived impulse response of 1 kHz filter when filtered MLS has been distorted with second-order nonlinearity at -10 dB. The spiky error can clearly be seen in the tail of the impulse response, and can be compared with the uncorrupted impulse response $h(n)$ of the lowpass filter in (a).

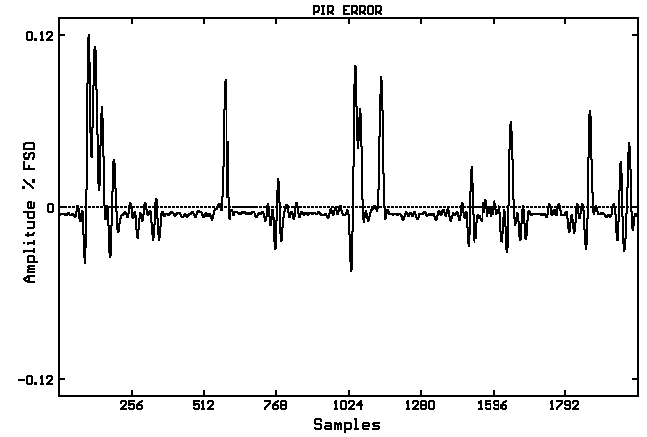

(a)

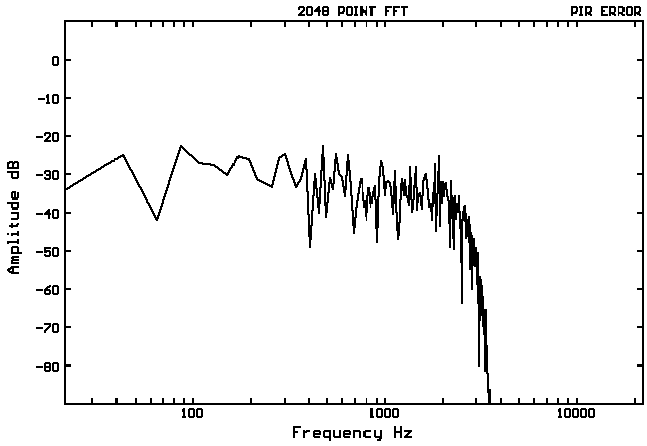

(b)

Fig. 8. MLS-derived impulse response error for 1 kHz FIR filter with second-order nonlinearity at -20 dB. (a) Time domain $e(n)$. (b) Frequency domain.

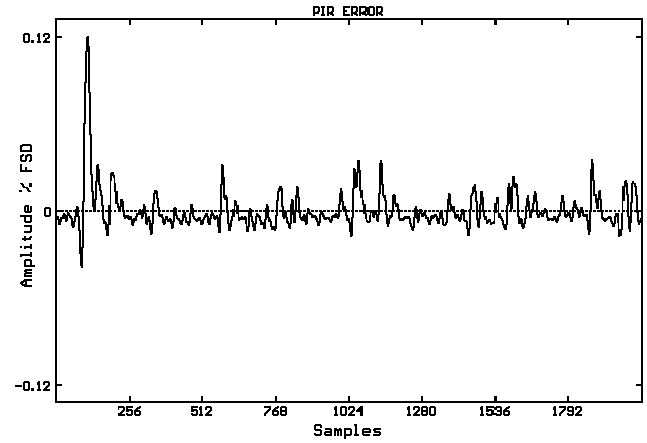

(a)

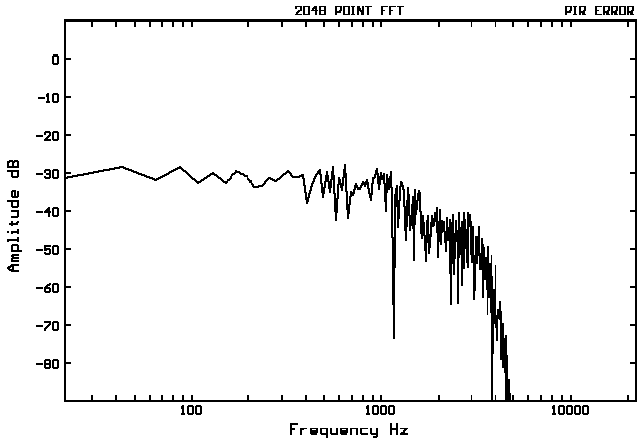

(b)

Fig. 9. MLS-derived impulse response error for 1 kHz filter and third-order nonlinearity. (a) Time domain $e(n)$. (b) Frequency domain.

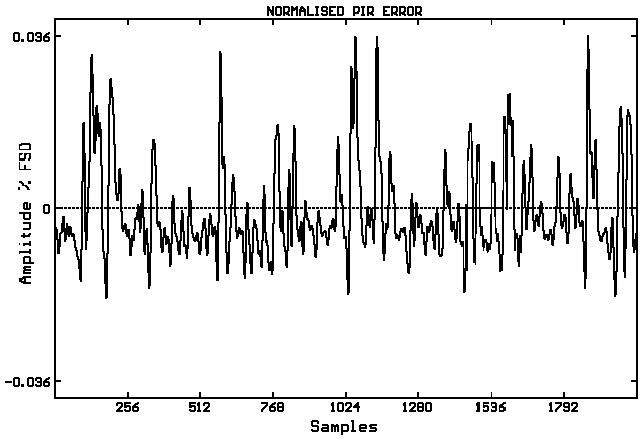

(a)

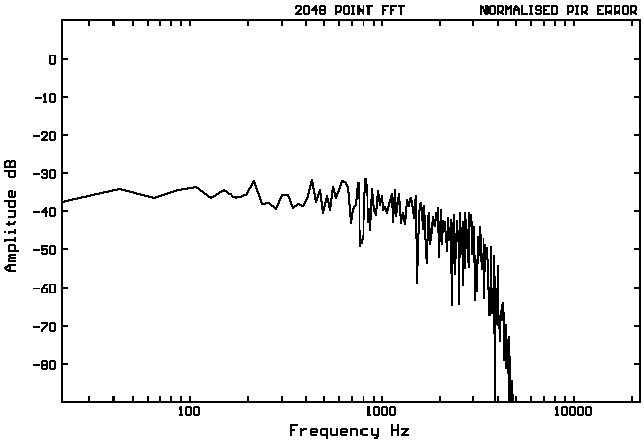

(b)

Fig. 10. MLS-derived nonlinear impulse response error (following error normalisation) for 1 kHz filter and third-order nonlinearity. (a) Time domain $e_{nl}(n)$. (b) Frequency domain.

3.3 Enhancing MLS Distortion Immunity by Truncation

We will now examine the effect that truncating a recovered impulse response has upon MLS distortion immunity. Rife and Vanderkooy [4] conjecture that distorting an MLS results in an MLS error sequence that can be viewed as a phase-randomised signal in the frequency domain which will, after cross-correlation, result in a recovered nonlinear impulse error $e_{nl}(n)$ that is evenly spread over the measurement period. This error distribution model will henceforth be referred to as the *constant error density model*. Since the linear impulse response $h(n)$ will typically be contained in the first few samples of the measurement, then truncating a measurement of period L at t samples should result in an increase in distortion immunity of T dB given by

$$T = 10 \log_{10} \left[\frac{L}{t} \right] \text{ dB} \quad . \tag{12}$$

To investigate the accuracy of the constant error density model some tests were performed upon the normalised error sequences $e_{nl}(n)$ obtained from the simulations. Fig. 11 shows the normalised error sequences and error distributions for distortion orders 2 through 5. The error distributions $P(n)$ are obtained by calculating error energy accumulation across the sequence as a proportion of total error energy after removing the DC error component,

$$P(n) = \frac{\sum_{k=0}^{n} \left[e_{nl}(k) - \frac{1}{L} \sum_{j=0}^{L-1} e_{nl}(j) \right]^2}{\sum_{k=0}^{L-1} \left[e_{nl}(k) - \frac{1}{L} \sum_{j=0}^{L-1} e_{nl}(j) \right]^2} \quad . \tag{13}$$

Hence for a constant error density, $P(n)$ should plot as a straight line from point 0, (0%) to point (L-1), (100%).

An examination of Fig. 11 indicates two trends:

(i) For similar orders of nonlinearity, even-order error distributions exhibit a greater degree of lumpiness than the odd-order distributions.

(ii) The distributions become smoother as the order of nonlinearity increases.

Further simulations with different MLS periods L (not shown here) have confirmed that these results are general. Hence the second-order error sequence will usually exhibit the lumpiest distribution; for the examples shown in Fig. 11, truncating the second-order measurement at 256 samples would increase distortion immunity by 4.5 dB rather than the 9 dB predicted by [Eq. (12)]. However, a truncation anywhere in the fifth-order error sequence will result in an increase in distortion immunity close to the predicted improvement, a result that is due to the smoother error distribution of the higher-order nonlinearity. The smoothing of error distribution with increasing order of nonlinearity is not surprising; the amplitude peaks in the filtered MLS will be accentuated by nonlinearity, and, for high-order distortion, tend to result in impulse-like transient errors in the distorted MLS. These transients result in an error sequence evenly spread across the recovered impulse response since cross-correlation with the unfiltered MLS $s(n)$ is equivalent to a time-reversed convolution with $s(n)$ (*i.e.* the error transients are convolved with $s(-n)$; see [4] for a more detailed discussion of transient noise immunity in MLS measurements).

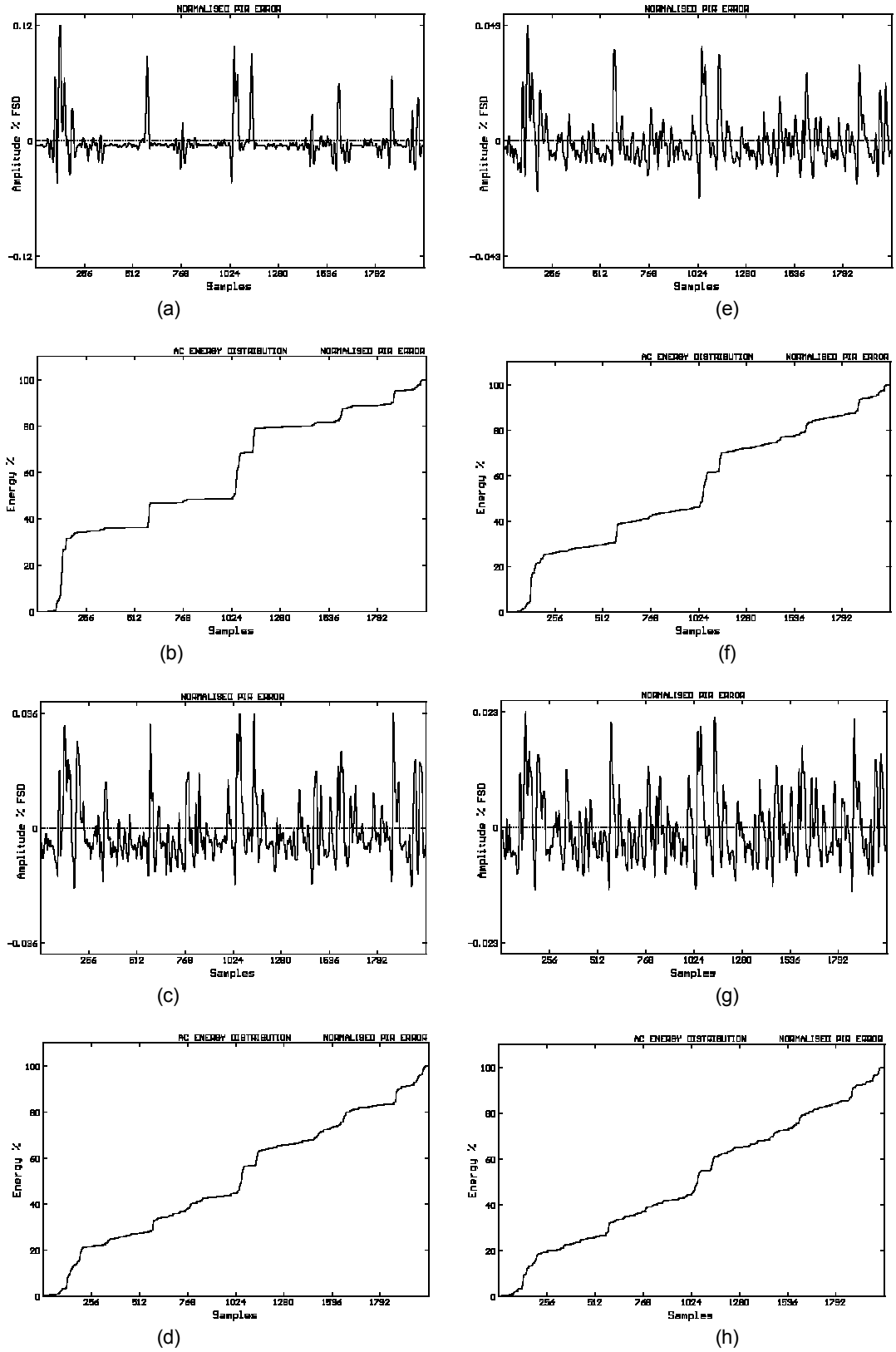

Fig. 11. Normalised nonlinear impulse response errors $e_{nl}(n)$ and error distributions $P(n)$ for MLS measurement of 1 kHz lowpass filter with (a), (b) second-, (c), (d) third-, (e), (f) fourth- and (g), (h) fifth-order nonlinearity.

It is important to note that, for low and particularly even-order nonlinearity, the increase in distortion immunity due to truncation is not necessarily *lower* than predicted by [Eq. (12)]. Depending on the particular MLS period used and the distortion order, it is also possible that the increase in distortion immunity will be higher than predicted. In general, the uneven error distributions introduce a degree of *uncertainty* to the improvement in distortion immunity gained from truncation. Since the degree of uncertainty in MLS error distribution is generally larger for even-order nonlinearity than for odd-order nonlinearity, a significant reduction in uncertainty is obtained by employing inverse repeat sequences (IRS), which exhibit complete immunity to even-order nonlinearity (see Sec. 6).

Rife and Vanderkooy also suggest that the error will tend to spread more evenly as the stimulus applied to the nonlinearity approaches a Gaussian amplitude distribution. The simulations so far have employed MLS signals filtered using a 1 kHz lowpass filter, resulting in a quasi-Gaussian amplitude distribution (Fig. 12). This can be compared to the MLS amplitude distribution shown in Fig. 13, obtained by lowpass filtering with a higher cutoff frequency (20 kHz), which is evidently *not* Gaussian. However, the impulse error distribution for the 20 kHz filtered MLS distorted with second-order nonlinearity [Fig. 14(b)] is very similar to the 1 kHz result shown in Fig. 11(b). Conversely the third-order error distribution for the 20 kHz filtered MLS [Fig. 14(d)] is less smooth than the 1 kHz result presented in Fig.11(d). These results suggest an ambiguous relationship between the filtered MLS amplitude distribution and error distribution.

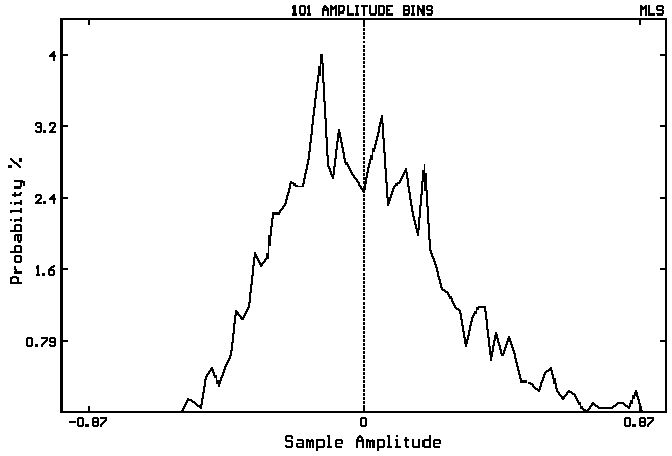

Fig. 12. Amplitude distribution for 1 kHz lowpass filtered MLS, showing almost Gaussian distribution

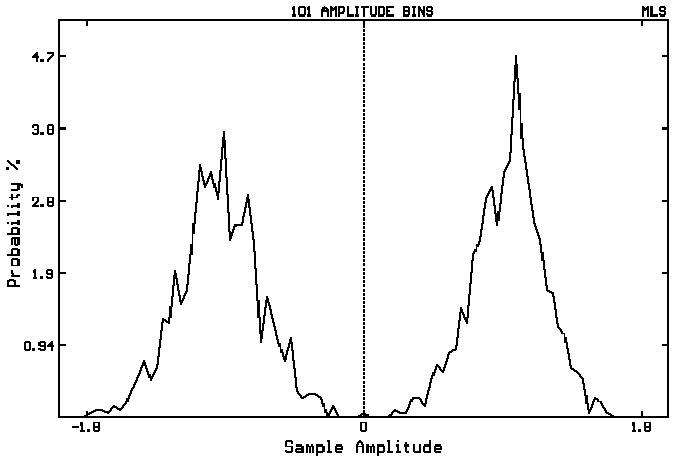

Fig. 13. Amplitude distribution for 20 kHz lowpass filtered MLS.

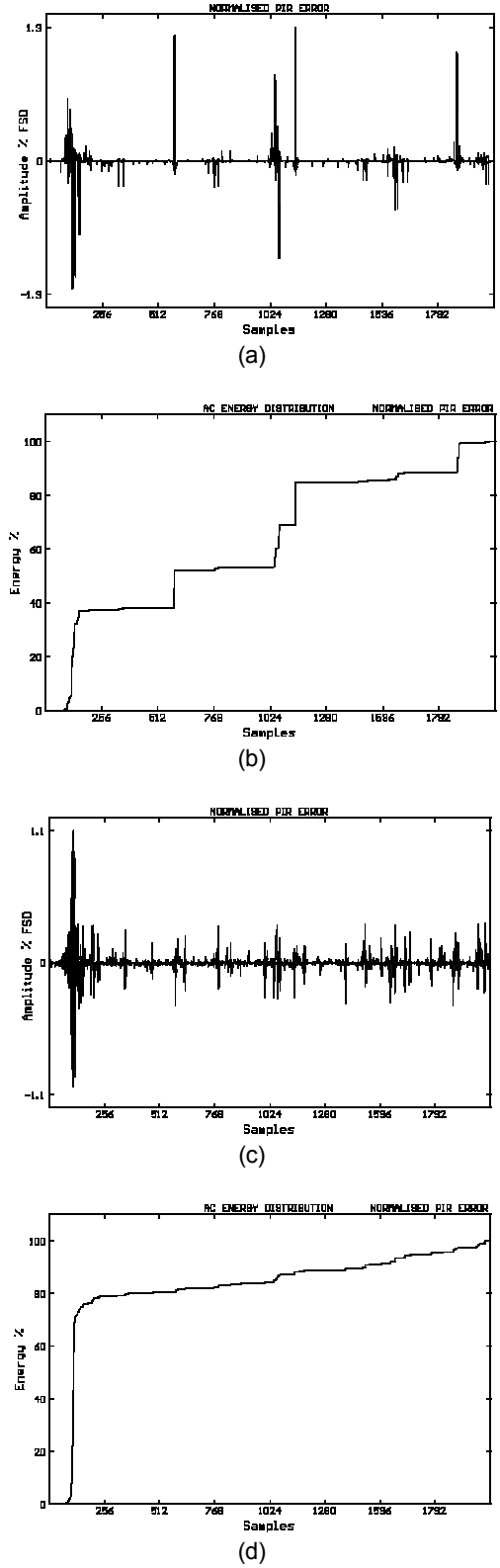

Fig.14. Normalised error sequence $e_{nl}(n)$ and error distribution $P(n)$ for MLS-derived impulse response of 20 kHz lowpass FIR filter with (a), (b) second-order memoryless nonlinearity and (c), (d) third-order memoryless nonlinearity.

Although we have so far used only memoryless distortion in our simulations, many physical nonlinear error mechanisms exhibit memory, *i.e.* where the current value of the error sequence depends upon previous values of the signal applied to the nonlinearity. Distortion mechanisms with memory usually exhibit frequency-dependent characteristics. In a private communication to the authors, Vanderkooy conjectures that MLS error sequence distributions due to nonlinearity with memory exhibit a degree of smoothing compared to the equivalent memoryless cases. In order to test this hypothesis we performed further simulations using a simple model for distortion with memory, where one argument to the nonlinearity is delayed by *b* samples. Hence for an *r*th-order nonlinearity,

$$d\{x_f(n)\} = A_d \left[\frac{x_f(n)}{x_{ref}} \right]^{r-1} \left[\frac{x_f(n-b)}{x_{ref}} \right] \quad . \tag{14}$$

The results of our simulations confirm that for *even*-order nonlinearity, memory in the distortion mechanism does tend to smooth error distributions. For example, Fig. 15(a) and (b) show the error sequence and distribution for second-order nonlinearity when b = 60; the plots can be compared to the memoryless error sequences in Fig. 11(a) and (b). However, for *odd*-order nonlinearity with memory, the linear gain error is delayed relative to $h(n)$ and is not removed during normalisation. This behaviour results in an error spike close to the linear impulse response, which cannot be removed by truncating the impulse response. Our simulations have indicated that the magnitude of the error spike is generally largest for third-order nonlinearity with memory, and for this case truncation will not yield large increases in distortion immunity. Fig. 15(c) and (d) show the error sequence and distribution for third-order nonlinearity with memory (b = 60), where 45 % of the total impulse response error energy is concentrated in the first 256 samples (12.5 %) of the measurement period.

Generally then the error distributions are evenly spread across the measurement period, a result which validates the constant error density model. Since noise artifacts will also be spread evenly across the measurement period, then MLS allows a basic separation of linear and error impulse response components. As we shall see in the next section, this behaviour is extremely useful in achieving optimal excitation amplitude.

4 OPTIMAL EXCITATION AMPLITUDE AND PERIOD IN MLS MEASUREMENTS

So far we have considered distortion immunity of MLS and PIE measurements, but real measurement environments will tend to suffer both distortion *and* noise corruption. In this section we ask: what is the *total* error immunity advantage of MLS over PIE, if any ? We will also examine methods of maximising total error immunity in practical MLS measurement systems, including selection of optimal excitation amplitude and measurement period.

4.1 Total Error Immunity Advantage of MLS over PIE

Rife and Vanderkooy [4] show that an unfiltered MLS has (L+1) times the signal power of a PIE at all signal frequencies bar DC when the peak signal voltage and sequence period are the same for both cases. This result is a direct consequence of the uniform spread of MLS excitation energy across the measurement period, compared to the localised (unit impulse) PIE signal. The noise power in a system is usually fixed in level (for example, room noise in a loudspeaker measurement). Thus the excitation signal-to-noise ratio in an MLS measurement is $10\log_{10}(L+1)$ dB higher than PIE. The energy conservation property of MLS cross-correlation [18] preserves the signal-to-noise ratio advantage of MLS through to the recovered impulse response. Thus MLS techniques possess a noise immunity advantage of approximately $10\log_{10}(L+1)$ dB over PIE, a result that is well known [4], [12], [19]. However, again compared to a PIE with equal (unfiltered) peak excitation amplitude, MLS has a distortion immunity *disadvantage* when measuring systems with bandwidths significantly lower than half the sampling frequency of the test system. In the following discussion we outline the reasons for this behaviour and argue that, broadly speaking, the *total* error immunity advantage shown by MLS is somewhat less than $10\log_{10}(L+1)$ dB.

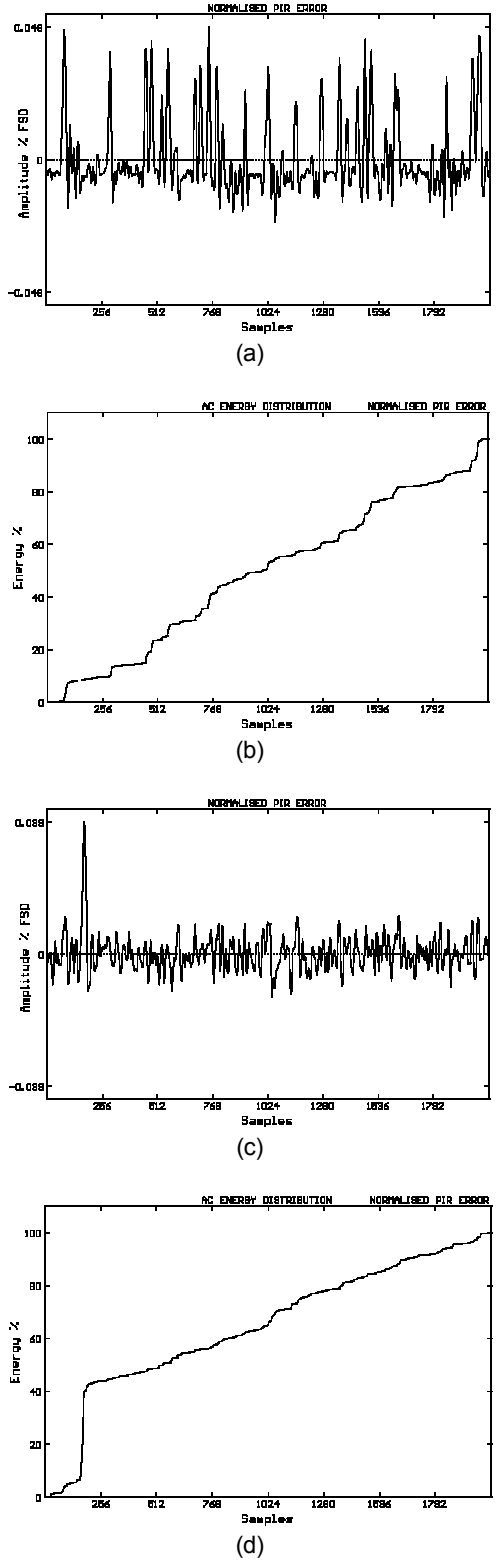

Fig. 15. Normalised error sequence $e_{nl}(n)$ and error distribution $P(n)$ for MLS-derived impulse measurement of 1 kHz FIR filter with (a), (b) second-order distortion with memory (delay b = 60 samples) showing smoothing of MLS error distribution compared to memoryless case, while (c), (d) third-order distortion with memory (delay b = 60 samples) indicates delayed gain error.

Consider a hypothetical system with a linear transfer function characterised by a unit impulse response, *i.e.* $h(n) = \delta(n)$. Applying either an MLS or PIE to such a system will result in an output signal unchanged from the input, *i.e.* for both cases the output signal has a binary amplitude distribution. Thus for equal peak input amplitudes and measurement periods, the `filtered' MLS and PIE signals possess identical peak voltages, although the MLS has (L+1) times the AC signal power of the PIE. If the filtered signals are now subject to memoryless nonlinearity, then the resultant MLS error signal will also have (L+1) times the power of the PIE error signal (ignoring for the moment the characteristics of the error signals). Because both the MLS signal and nonlinear error powers are (L+1) times the respective powers for PIE, the distortion immunities for the two stimuli are equal. Again this is a direct consequence of the energy conservation property of MLS cross-correlation. Now consider what happens when the main lobe of the system impulse response broadens over at least a few samples, for example when the system bandwidth is lower than half the measurement system sampling frequency. If the peak input excitations and the measurement periods are again equal, the filtered excitation will tend to have a higher peak voltage for MLS compared to PIE. This occurs because `runs' of successive 1's and -1's in the unfiltered MLS stimulus [20] effectively integrate the system impulse response over regions of the measurement period during convolution, whereas for PIE the system is stimulated for one sample only. This behaviour is illustrated by comparing the peak voltage for the 1 kHz filtered PIE [Fig. 3(a)] to that of the 1 kHz filtered MLS [Fig. 7(b)]; note the change in vertical axis scaling. The higher peak voltage of the filtered MLS stimulates any nonlinearity more vigorously than for PIE, hence the error energy within the filtered and distorted MLS is greater than (L+1) times the error energy encountered in PIE. Consequently MLS has a lower excitation signal-to-distortion ratio than PIE, and hence a distortion immunity disadvantage for the lower system bandwidth. As the system bandwidth increases and the system impulse response approaches a unit impulse, then the MLS distortion immunity disadvantage decreases, eventually becoming zero when the test system impulse response is equal to a unit impulse.

Two examples that help to illustrate this behaviour are presented in Tables 1 and 3, where the distortion immunities of (untruncated) MLS-derived impulse responses are compared to PIE measurements for memoryless nonlinearities ranging from second to seventh order. Both the unfiltered peak amplitude prior to filtering and the measurement period (L = 2047) are constant throughout the MLS and PIE simulations. Table 1 compares the distortion immunities for the two methods with 1 kHz FIR filtering, indicating a clear disadvantage for MLS under these conditions with all distortion orders. MLS distortion immunity disadvantage remains evident when the filter cutoff frequency is increased to 10 kHz (Table 3), although the disadvantage is now reduced somewhat (as predicted). MLS distortion immunity disadvantage under these excitation conditions must be weighed against the improved noise performance compared to PIE which, for L = 2047, will equal 33.1 dB. The question now posed is, what is the effect of varying the excitation amplitude upon the relative noise and distortion immunities of the two methods ?

For any transfer function measurement strategy and simple distortion mechanisms described by Eq. (2), the error due to nonlinearity increases as the peak level of the excitation increases, although the rate at which the error increases depends upon the order of nonlinearity that the test system is subject to. A 6 dB increase in driving level will *decrease* distortion immunity by 6 dB for second-order nonlinearity, 12 dB for third-order, and so on. If the increase in peak unfiltered excitation amplitude is ΔA dB, then we can write

$$\Delta I_d = -(r-1)\Delta A \quad . \tag{15}$$

For system noise that is fixed in level, the noise immunity will *increase* by 6 dB for every 6 dB increase in excitation amplitude. If I_n represents noise immunity in dB, then

$$\Delta I_n = \Delta A \quad . \tag{16}$$

We can use Eqs. (15) and (16) to predict the noise immunity advantage of MLS over PIE following distortion immunity normalisation. Consider the third-order result from Table 1 where, for equal unfiltered peak excitation amplitudes, PIE has a distortion immunity of 77.2 dB while MLS offers 35.4 dB. To make the distortion immunities for both techniques equal to 77.2 dB, the MLS excitation amplitude must be reduced. Using Eq. (15), the required reduction in amplitude is (77.2 - 35.4)/2 = 20.9 dB. Reducing the

MLS excitation amplitude by this amount yields a reduced noise immunity advantage for MLS; using Eq. (16) the new MLS noise immunity advantage is (33.1 - 20.9) = 12.2 dB. This procedure was followed for all of the examples listed in Tables 1 and 3, and the new noise immunity results recorded in Tables 2 and 4 respectively. These predicted results were found to agree identically with a further set of MLS simulations performed at the lower excitation amplitudes. Generally it is clear that some degree of MLS noise immunity advantage remains following distortion immunity normalisation, although the noise immunity advantage is then not as high as $10 \log_{10}(L+1)$ dB.

How can we use this information to predict the *minimum* total error immunity advantage of MLS over PIE ? The answer to this question evidently depends upon the relative levels of noise and distortion present in the test environment. For a system with low levels of weak nonlinearity the noise error will dominate and total error immunity will be limited by the peak amplitude allowed in the system before overload. In this case MLS will show a $10 \log_{10}(L+1)$ dB total error immunity advantage over PIE. Most systems however will exhibit some degree of noise *and* distortion error. For these situations there will be some optimum driving level where the error contributions due to noise and distortion are equal and together result in the highest possible overall error immunity. When the driving signal is increased above this optimum level the distortion error will dominate, while noise will be dominant for lower signal levels. If MLS still offers a noise immunity advantage over PIE when distortion immunities for both techniques are equal, then a little thought reveals that MLS must also possess some degree of total error immunity advantage over PIE when driving levels are optimised individually for both cases. Generally we can state that given the same measurement period L but optimal excitation amplitudes, MLS offers a total error immunity advantage over PIE of between 0 dB and $10 \log_{10}(L+1)$ dB, the exact advantage depending on (i) the relative levels of noise and distortion in the test system and (ii) the sampling frequency employed for the measurement. We have seen that with normalised distortion immunities, MLS noise immunity advantage tends to increase as the bandwidth of the DUT increases relative to the sampling frequency of the test system. Hence the greatest overall error immunity advantage offered by MLS over PIE for a given DUT occurs when the MLS/PIE sampling rate is as low as possible.

The arguments presented so far are based upon measurements where the recovered impulse response remains untruncated. As we have seen in Sec. 3, truncation will yield enhancements in distortion immunity for MLS where impulse error due to nonlinearity is generally evenly spread across the measurement period. Noise immunity will also be improved by truncation for both MLS and PIE, since the noise error is spread evenly across the measurement period for both techniques. However, nonlinear errors in PIE measurements are coincident with the linear impulse (Figs. 3, 4, 5) and thus PIE distortion immunity will not be increased by truncation. Thus for a system prone to both noise and distortion, truncation improves the minimum total error immunity advantage of MLS over PIE. We should also note that we have characterised nonlinearity in the measurement system by simple power laws [see Eq. (2)], although many practical systems also suffer from other types of nonlinearity. For example, ADC quantisation distortion can corrupt the data acquisition stage of measurement, while crossover distortion and slew limiting can occur in power amplifiers used to drive loudspeakers under test. To a first-degree approximation, both quantisation distortion and crossover nonlinearity remain fixed in level as the excitation amplitude is varied. These errors can therefore be treated as system noise and do not change the basic arguments presented earlier. For a full discussion of the effects of slew limiting in MLS measurements we refer the reader to Godfrey and Murgatroyd [10] and Vanderkooy [11].

4.2 Determining Optimal Excitation Amplitude

We have seen that, given optimal excitation amplitudes for both techniques, MLS measurements theoretically exhibit at least some degree of overall error immunity advantage over PIE. However, practical PIE measurements have a further disadvantage since it is often difficult to achieve optimal excitation amplitude. First, the driving signal energy is relatively low so that the effects of distortion are often negligible in comparison to the noise error. The driving system (for example, the power amplifier in a loudspeaker PIE measurement) is often overloaded before the optimal driving amplitude is achieved.

Second, there is the problem of effectively monitoring the error due to nonlinearity in PIE measurements, because the linear impulse and nonlinear error signals are coincident in the time domain. Conversely, MLS allows the overall error level to be easily monitored by windowing the tail of the recovered impulse response, which given a sufficiently long measurement period will contain only noise and distortion error components (see Sec. 3). Optimal MLS excitation amplitude is achieved when there is minimal energy in the tail of the impulse response with respect to the energy of the linear (initial) part of the impulse response. This is equivalent to maximising the MLS coherence function proposed by Rife and Vanderkooy [4]. Consider Fig. 16 which show the last 1023-points of the recovered impulse responses from simulated MLS measurements which have been corrupted by nonlinearity (third order) and Gaussian noise. Remembering that the amplitude scaling in the time-domain plots is relative to the peak level of the driving signal, Fig. 16(a) shows the impulse tail when the driving level is 6 dB too high and distortion artifacts dominate the error signal. Optimal error immunity is achieved in Fig. 16(b) by reducing the MLS amplitude by 6 dB which results in noise and distortion errors of equal energy. The overall error immunity is increased by about 9 dB over Fig. 16(a). When the driving level is further reduced by 6 dB in Fig. 16(c), noise now dominates and overall error immunity is reduced by approximately 3 dB from the optimal arrangement of Fig. 16(b).

4.3 Selecting Optimal Measurement Period

Given that we can determine the optimal excitation amplitude in an MLS measurement by examining the tail of the recovered impulse response, what is the best MLS period L to use ? Although we have only presented results for L = 2047, additional simulations with L ranging from 255 to 8191 samples have indicated that MLS noise and distortion immunity for a given DUT both remain fairly constant as L changes. If the MLS period is much longer than the length of the impulse response being measured then noise and distortion immunity can both be substantially increased by discarding the tail of the recovered PIR, because as we have seen in Sec. 3, both the error due to noise and that due to distortion are evenly distributed across the measurement period. Of course the increase in noise immunity obtained from such a truncation could also be effected by averaging several shorter measurements, but averaging has no effect upon distortion immunity, and the single long MLS measurement ultimately takes less time to execute. Thus we conclude that for maximum overall error immunity the period of MLS measurements should be made as large as possible, and the PIR recovered from cross-correlation should be truncated to as short a length as possible.

5 CUMULATIVE SPECTRAL DECAY PLOTS OF WEAKLY NONLINEAR SYSTEMS

In general, impulse response corruption due to nonlinearity will also corrupt information derived from the basic impulse response data. For example, Vanderkooy [11] has studied the effect of nonlinearity upon reverberation plots obtained from MLS measurements. In this section we examine the effect that weak nonlinearity has upon the accuracy of cumulative spectral decay (CSD) plots generated from impulse response measurements. Examples illustrate the increases in decay plot resolution to be gained from optimising stimulus amplitude in the impulse response measurement.

CSD or "waterfall" plots indicate how linear systems respond to tone bursts. Their use is becoming more widespread in loudspeaker evaluation [8], [9] because they allow a simple analysis of delayed resonances. An appropriately apodized CSD plot $C_a(\tau,\upsilon)$ is generated using the following function:

$$C_a(\tau,\upsilon) = \mathrm{F}\{h(t)\, w(t,\tau)\} \quad , \tag{17}$$

where
- τ is the time variable of the plot;
- υ is the frequency variable of the plot;
- F is the Fourier operator;
- $h(t)$ is the impulse response of the DUT;
- $w(t,\tau)$ is a window function which influences the time and frequency resolution of the generated plot.

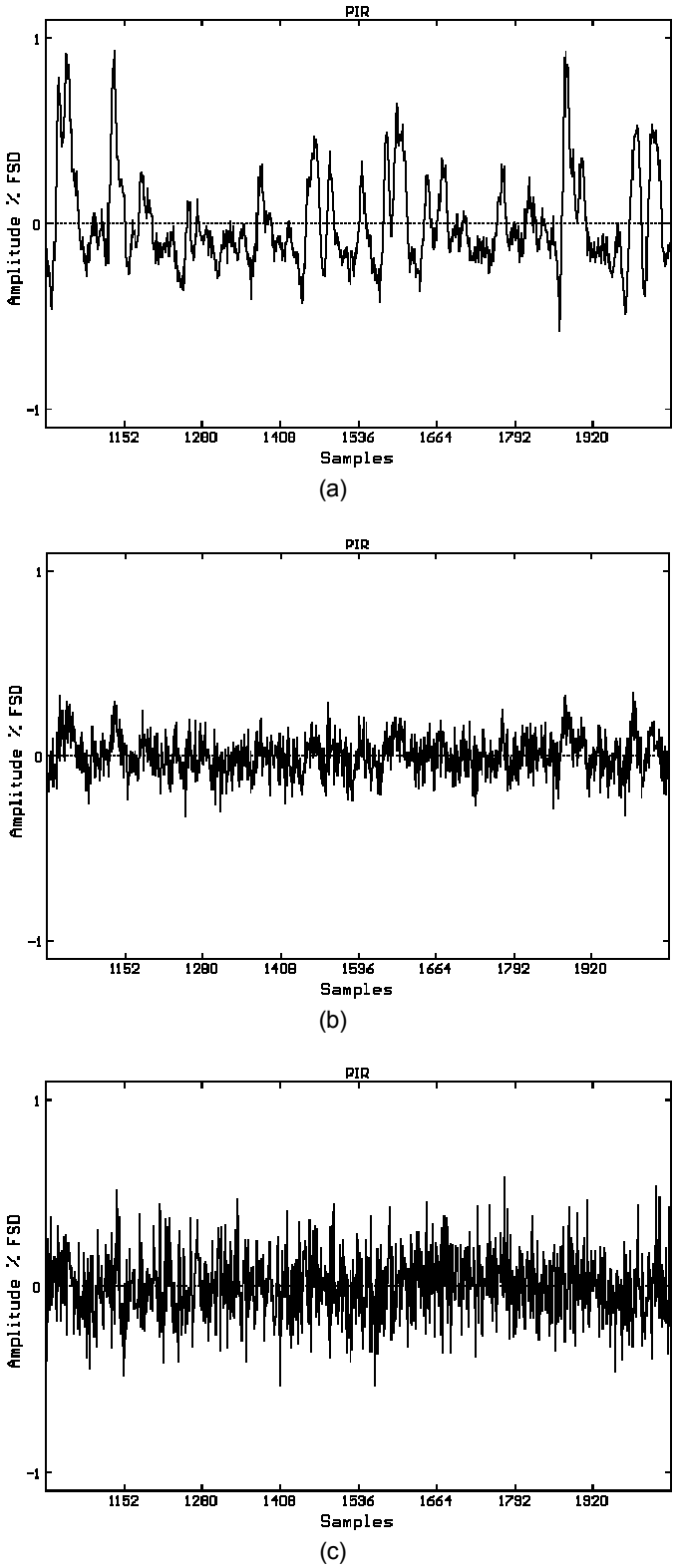

Fig. 16. Tail of impulse response from noisy and nonlinear MLS measurements. (a) MLS amplitude 6 dB too high; third-order distortion artifacts dominate. (b) Optimal excitation amplitude; noise and distortion powers are equal. (c) MLS amplitude 6 dB too low; noise dominates.

For a full discussion of CSD plots we refer the reader to [21] and [22]. Following the conventions established in these works, the simulations presented below were generated using a raised-cosine window function with a rise time *at* of 0.5 ms, fixed window time *wt* of 3.5 ms and a fall time *dt* of 2 ms [Fig. 17(a)]. The 0 ms graduation on the decay plot time axes corresponds to the peak of the impulse response under evaluation. Fig. 17(b) indicates the spectral decay of a 20 kHz lowpass FIR filter. Apart from the characteristic FIR structure ringing around 20 kHz, this waterfall diagram shows a rapid energy decay across the audio band. Now consider Fig. 17(c), which shows the cumulative spectral decay of the same filter using a PIE-derived impulse response corrupted by second-order nonlinearity. Other than some additional high frequency energy above 20 kHz the plot is very similar to that of the linear filter plotted in Fig. 17(b). This behaviour is expected since nonlinear artifacts in a PIE measurement are concentrated in the vicinity around the linear impulse response (see Sec. 2), and the error component therefore falls outside the analysis window after the first few CSD sections. However, this is not true of an MLS-based measurement, where we have seen in Sec. 3 that error due to nonlinearity is spread evenly over the entire measurement period. Here the error will effect the cumulative spectral decay right across the plot and will be especially influential towards the front of the diagram where the main impulse energy has fallen outside the analysis window. This behaviour is illustrated in Fig. 17(d) where the waterfall has been generated from an MLS measurement with second-order nonlinearity. After the initial energy decay, nonlinear artifacts within the analysis window cause ripples in the decay plot which could be mistaken for delayed resonances attributable to the *linear* characteristics of the DUT. Similar errors occur in both MLS and PIE measurements that are corrupted with noise (which is, of course, evenly spread across the measurement period for both techniques). Indeed, poor noise immunity in PIE measurements can severely limit the resolution obtained from PIE-derived decay plots, and the advantages that MLS measurements possess in terms of total error immunity once optimal excitation amplitude is established are of real benefit here. An example used to illustrate the benefits of optimising excitation levels in an MLS-derived decay plot is presented in Fig. 18, where white Gaussian noise and fourth-order nonlinearity corrupt impulse response measurements of the 20 kHz FIR filter used for the simulations of Fig. 17. The sequence of excitation conditions is similar to that of Fig. 16, *i.e.* we examine the plots obtained from measurements where the driving amplitude is 10 dB too high [Fig. 18(a)], followed by optimal excitation amplitude [Fig. 18(b)], and finally an amplitude which is 10 dB below optimum [Fig. 18(c)]. In Fig. 18(a) the error due to nonlinearity severely corrupts the decay plot, while in Fig. 18(c) noise is largely responsible for the decay plot error. The decay plot shown in Fig. 18(b) clearly possesses the lowest error component, a condition which is coincidental with optimal excitation amplitude being achieved. Although this is a slightly contrived example in that the use of high-order nonlinearity accentuates the increase in total impulse response error when the excitation amplitude is too high, it does illustrate the gains to be made from optimising excitation conditions. It is interesting to compare the decay plot obtained from the optimal MLS measurement [Fig. 18 (b)] to that obtained from an optimal PIE stimulus (Fig. 19). The total error immunity advantage of MLS is clearly evident.

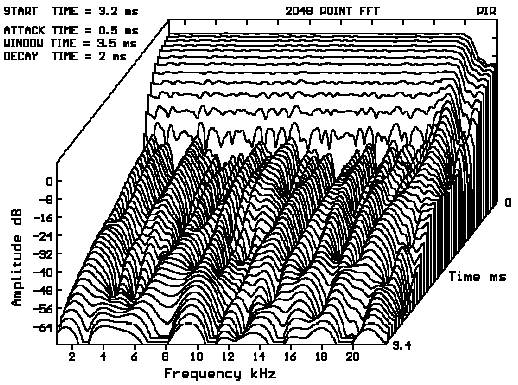

Fig. 19. Decay plot obtained from PIE-derived impulse response measurement of 20 kHz FIR filter. Measurement is corrupted with white Gaussian noise and fourth-order nonlinearity, while PIE excitation amplitude is optimal.

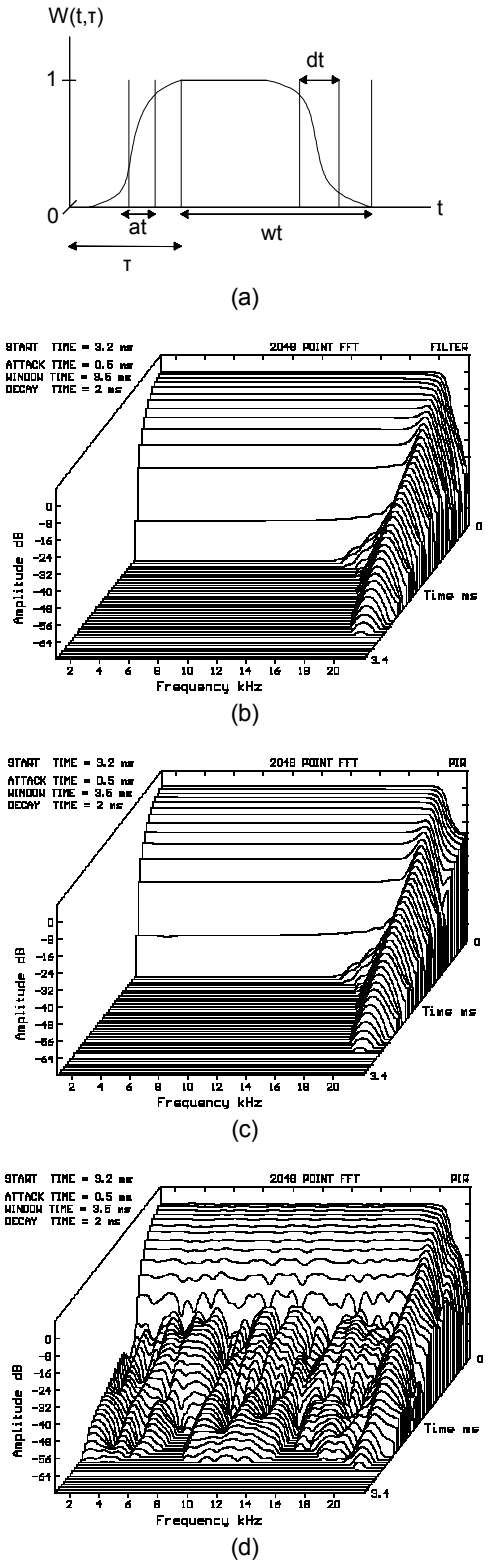

Fig. 17. Effects of nonlinearity upon cumulative spectral decay plots. (a) Window function $w(t,\tau)$. (b) Decay plot of 20 kHz FIR filter. (c) Decay plot of impulse response from distorted PIE measurement. (d) Decay plot from distorted MLS measurement.

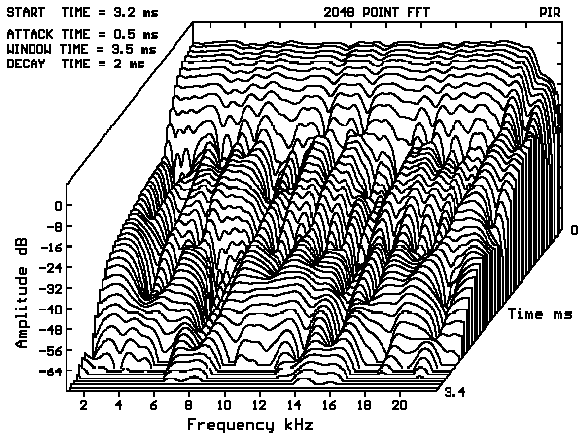

(a)

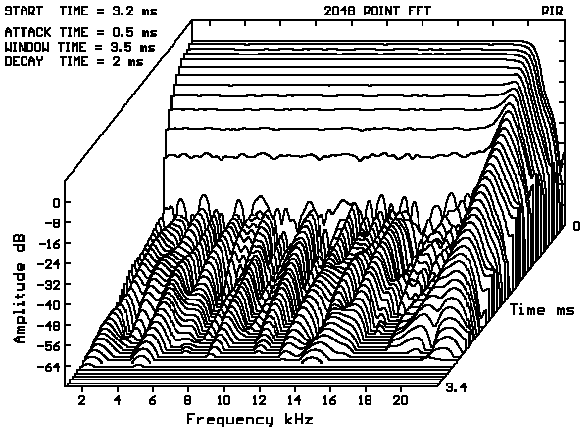

(b)

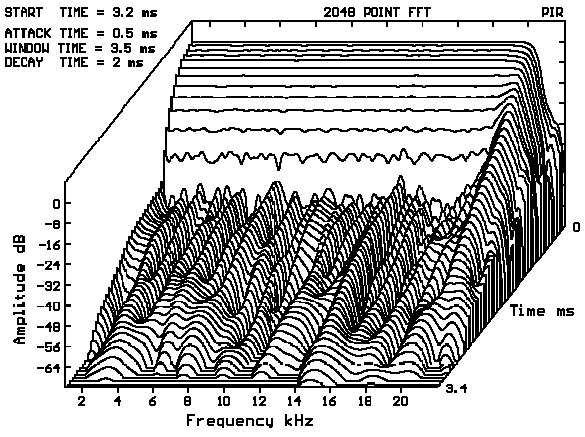

(c)

Fig. 18. Effect of optimising excitation amplitude in cumulative decay plots derived from MLS impulse response measurements of 20 kHz FIR filter corrupted with white Gaussian noise and fourth-order nonlinearity. (a) Excitation amplitude 10 dB too high; nonlinear error dominates. (b) Optimal excitation amplitude, resulting in minimal plot corruption. (c) Excitation 10 dB too low, where noise error dominates.

6 INVERSE REPEAT SEQUENCES

Referring to our nonlinear system model [Fig. 2(c)], consider the error signal $d\{x_f(n)\}$ due to a second-order nonlinearity:

$$d\{x_f(n)\} = A_d[x_f(n)]^2 \quad . \tag{18}$$

Now

$$\begin{aligned} x_f(n) &= x(n) \otimes h(n) \\ &= \sum_{i=0}^{L-1} h(i)\, x(n-i) \ . \end{aligned} \tag{19}$$

Combining Eqs. (18) and (19) yields

$$d\{x_f(n)\} = A_d \sum_{i=0}^{L-1} \sum_{j=0}^{L-1} h(i)\, h(j)\, x(n-i)\, x(n-j) \ . \tag{20}$$

When the input signal is an MLS, then $x(n) = s(n)$ and the impulse error $e(n)$ is obtained by cross-correlating $d\{x_f(n)\}$ with $x(n)$ [as in Eq. (11)]:

$$\begin{aligned} e(n) &= x(n) \ \Phi \ d\{x_f(n)\} \\ &= \frac{1}{L+1} \sum_{k=0}^{L-1} x(k)\, d\{x_f(n+k)\} \\ &= \sum_{i=0}^{L-1} \sum_{j=0}^{L-1} A_d\, h(i)\, h(j) \left[\frac{1}{L+1} \sum_{k=0}^{L-1} x(k)\, x(k+n-i)\, x(k+n-j) \right] \\ &= \sum_{i=0}^{L-1} \sum_{j=0}^{L-1} A_d\, h(i)\, h(j)\, \Omega_2(n-i,\, n-j) \quad . \end{aligned} \tag{21}$$

Here Ω_2 is the second-order autocorrelation of the unfiltered MLS. We can write Eq. (21) in more general terms as a function of the second-order *kernel* of the system $h_2(i, j)$, of which our memoryless second-order nonlinearity is a specific case, *i.e.*

$$h_2(i, j) = A_d\, h(i)\, h(j) \ . \tag{22}$$

Generalising Eq. (21) to include a number of nonlinear kernels yields

$$\begin{aligned} e(n) = & \sum_{i=0}^{L-1}\sum_{j=0}^{L-1} h_2(i,j)\,\Omega_2(n-i,n-j) \\ & + \sum_{i=0}^{L-1}\sum_{j=0}^{L-1}\sum_{k=0}^{L-1} h_3(i,j,k)\,\Omega_3(n-i,n-j,n-k) \\ & + \sum_{i=0}^{L-1}\sum_{j=0}^{L-1}\sum_{k=0}^{L-1}\sum_{l=0}^{L-1} h_4(i,j,k,l)\,\Omega_4(n-i,n-j,n-k,n-l) \\ & + \ldots \end{aligned} \tag{23}$$

Each term in Eq. (23) is an r-dimensional convolution of a system kernel $h_r(n_1, n_2, ..., n_r)$ with the appropriate autocorrelation function $\Omega_r(n_1, n_2, ..., n_r)$ of the input sequence, where

$$\Omega_r(n_1, n_2, \ldots n_r) = \frac{1}{L+1}\sum_{k=0}^{L-1} x(k)\,x(k+n_1)\,x(k+n_2)\ldots x(k+n_r) \quad . \tag{24}$$

Using the shift and add property of MLS signals [23] it is easy to show that Ω_r can only take on two values, $L/(L+1)$ (a `spike') and $-1/(L+1)$. It is the spikes in Ω_r that cause the spikiness in the impulse error sequence $e(n)$ that we noted in Sec. 3.2. Following arguments similar to those presented in [24] it can be shown that there are approximately L^{r-1} spikes in Ω_r, evenly distributed across the L^r co-ordinates of the r-dimensional autocorrelation function. It is the even distribution of spikes in Ω_r which causes $e(n)$ to be evenly distributed across L, as we have seen in Sec. 3.3.

Now consider a periodic binary signal $x(n)$ suitable for impulse response measurement, where the second half of the sequence is the exact inverse of the first half, *i.e.*

$$x(n+L) = -x(n) \quad . \tag{25}$$

Note that the period $2L$ of such a sequence will always contain an even number of samples. Referring to Eq. (24) and extending the limits of the summation to $2L$-1, all even-order autocorrelations (r even) will be exactly zero, simply because for all $n_1, n_2 \ldots n_r$, each $x(k)x(k+n_1)\ldots x(k+n_r)$ term within the summation will exactly cancel with the corresponding $x(k+L)x(k+L+n_1)\ldots x(k+L+n_r)$ term. Such a sequence would therefore also possess complete immunity to even-order nonlinearity after cross-correlation. Due to the anti-symmetry in $x(n)$ the first-order autocorrelation will also possess anti-symmetry about L, *i.e.* $\Omega_1(n) = -\Omega_1(n+L)$. It is desirable that $x(n)$ be chosen such that the first half of Ω_1 is as close to a unit impulse as possible so that the linear impulse response of the DUT can be easily measured by cross-correlating the system output with input (the second inverted half of the cross-correlation can simply be discarded). A signal that satisfies these conditions is the so-called `inverse repeat sequence' (IRS), obtained from two periods of an MLS where every other sample of the MLS is inverted [24], *i.e.*

$$\begin{aligned} x(n) &= s(n) \qquad n \text{ even}, \quad 0 \le n < 2L \\ &= -s(n) \qquad n \text{ odd}, \quad 0 < n < 2L \quad . \end{aligned} \tag{26}$$

where L is the period of the generating MLS (note that the IRS period is $2L$). A 62-point IRS generated from a 31-point MLS (5 stage shift register) is shown in Fig. 20(a). The first-order autocorrelation of an IRS Ω_{IRS1} is related to the corresponding signal for the generating MLS by the following expression:

$$\begin{aligned}\Omega_{IRS1}(n) &= \frac{1}{2(L+1)}\sum_{k=0}^{2L-1} x(n)x(n+k) \\ &= \Omega_{MLS1}(n), \quad n \text{ even} \\ &= -\Omega_{MLS1}(n), \quad n \text{ odd} \\ &= \delta(n) - \frac{(-1)^n}{L+1} - \delta(n-L), \qquad 0 \le n < 2L.\end{aligned} \tag{27}$$

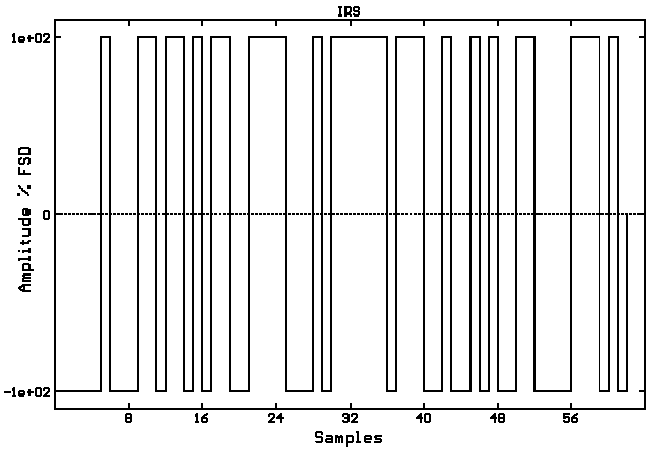

(a)

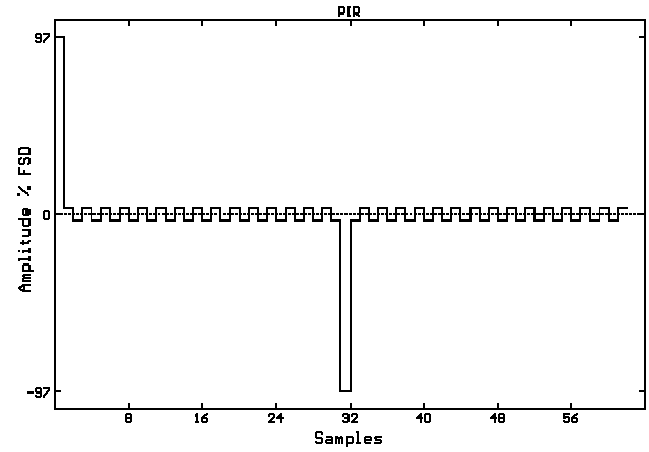

(b)

Fig. 20. (a) IRS formed from fifth-order MLS. (b) Autocorrelation sequence.

The first-order autocorrelation for the 62-point IRS is shown in Fig. 20(b), clearly showing anti-symmetry about L. There is also a small term oscillating at a rate of half the sampling frequency due to the $(-1)^n/(L+1)$ factor in Eq. (27). The power spectrum of a periodic sampled signal is defined as the discrete Fourier transform (DFT) of its autocorrelation, thus the IRS is spectrally flat at all frequencies except for DC and half the sampling frequency where the power is exactly zero. In a practical measurement system this would not be of concern because many systems such as loudspeakers do not possess a magnitude response that extends to DC, while the ADC used to digitise the system output signal will usually employ

an antialiasing filter which will reject all information at half the sampling frequency. Thus by exciting a linear system with an IRS, sampling the output of the system and cross-correlating that output with the (known) unfiltered IRS we obtain the impulse response of the system in much the same way that we would if using an MLS excitation. Of course the antisymmetry in the IRS autocorrelation results in an inverted copy of the system impulse response beginning at L samples. For example, Fig. 21 shows the recovered impulse response from a simulated 4094-point IRS measurement of the 1 kHz FIR filter. Since the second half of the cross-correlation contains no additional information, it can simply be discarded.

We have shown that impulse response measurements from IRS signals offer complete immunity to even-order nonlinearity. However, for odd-order distortion the recovered impulse response will still contain an error component, although, like MLS, this error component will tend to be spread evenly across the measurement period after error normalisation. Fig. 22(a) shows the nonlinear error component for third-order nonlinearity at -20 dB with the 1 kHz lowpass FIR filter. This figure can be compared directly with Fig. 11(c), which shows the equivalent MLS error sequence. The most obvious difference is that the IRS error sequence has bipolar spikes. This is because the odd-order autocorrelation functions for an IRS can assume 4 levels, ± 1 and ± 1/(L+1), whereas we have seen that MLS autocorrelation functions are two valued. For an IRS the spikes appear in ±1 pairs, and so for low-bandwidth systems, where the system kernels $h_r(n_1,n_2,...n_r)$ change slowly across r-dimensional space, some of the spike pairs tend to partially cancel out in the cross-correlation operation [Eq. (23)]. This behaviour results in an increase in distortion immunity for low-bandwidth systems (compared with the equivalent MLS case).

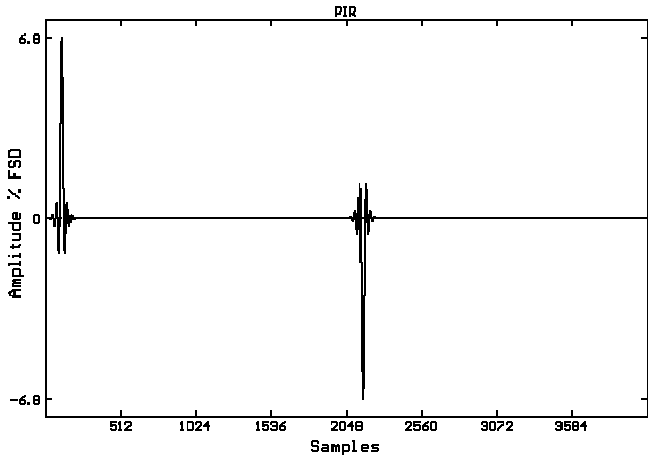

Fig. 21. Output of IRS crosscorrelation indicating anti-symmetry about L samples.

In order to determine IRS distortion immunity, simulations were performed with various nonlinearities using a process similar to that used for the MLS simulations [Eq. (11)]. MLS convolution and cross-correlation routines take advantage of the FHT as discussed in Sec. 3, and in principle there is no reason why IRS convolution and cross-correlation cannot also be performed using the FHT. However, permutation routines that make the most efficient use of the FHT (as developed by Borish for MLS) are not yet available for IRS. Hence for the IRS simulations all convolutions and crosscorrelations were performed by FFT in the frequency domain. Because the number of samples in an IRS period is not an exact power of 2, double-length FFTs must be used with zero padding (see chapter 12 of [25]). The results of IRS distortion immunity simulations for second- to seventh-order nonlinearity with the 1 kHz FIR filter are tabulated in Table 1. Distortion immunity for even-order nonlinearity is extremely high and is only limited by the accuracy of the calculations in the simulations at approximately -250 dB (lower than MLS simulation accuracy because of the sizeable increase in the number of computational operations required for the IRS simulations) . For odd-order nonlinearity the IRS excitation shows a small increase in distortion immunity over MLS. This is not true for higher bandwidth simulations tabulated in Table 3. Here the FIR lowpass filter now has a cutoff frequency of 10 kHz and IRS odd-order distortion immunity can be seen to

be identical to MLS. Finally we should note that, like MLS, IRS impulse response error due to nonlinearity is generally evenly spread across the measurement period [Fig. 22(b)]. Thus an IRS impulse measurement will also show an increase in distortion immunity after truncation. A point worth noting is that the second half of the autocorrelation output is the *exact* inverse of the first half, including any artifacts due to noise or distortion. Hence IRS error immunity is in no way affected by subtracting the second half of the recovered antisymmetric impulse response from the first half.

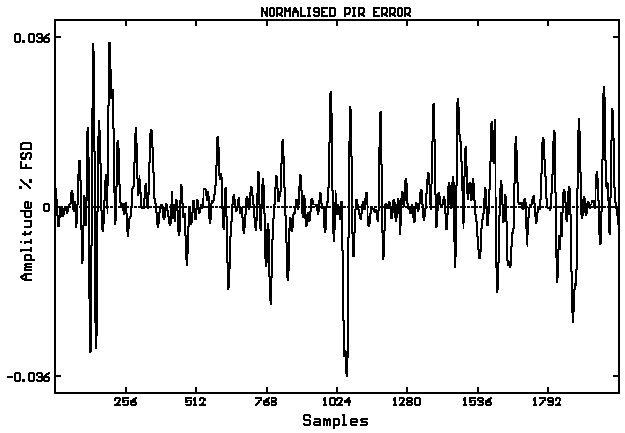

(a)

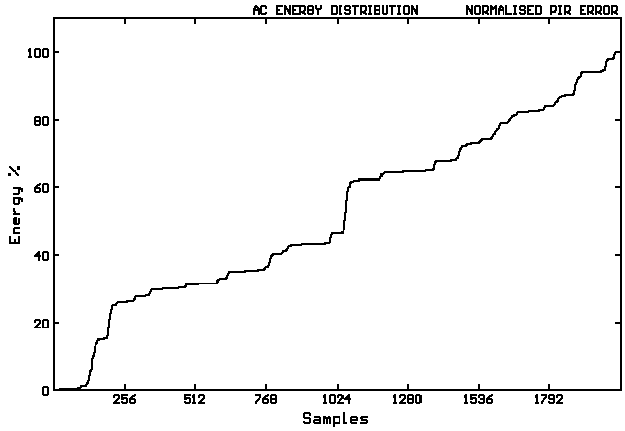

(b)

Fig. 22. (a) Normalised nonlinear impulse error $e_{nl}(n)$ and (b) error distribution $P(n)$ from IRS-derived impulse response measurement of 1 kHz FIR filter with third-order nonlinearity.

Inverse repeat sequences thus possess an impressive distortion immunity advantage over MLS and, given that the basic theory has been known for some time [24], [26], [27], it is surprising that IRS techniques are not in more widespread use. Are there any disadvantages suffered by IRS measurements? Obviously for an L-point impulse response measurement, $2L$ samples must be generated, stored in memory and then cross-correlated. There is no difficulty in generating the inverse repeat sequence since this can be formed using a shift register in a similar fashion to MLS. However, given a memory limit in a practical measurement arrangement, MLS will recover an impulse response that is twice as long as that available from IRS. For impulse lengths found in typical test devices such as loudspeakers, this does not represent a problem. Since an IRS of period $2L$ will have the same noise immunity as an MLS of length $(2L+1)$, there is also no penalty to pay in terms of maximum noise immunity. There is, however, a disadvantage in cross-correlation time for IRS when employing an FFT-based cross-correlation algorithm. If we assume that the execution time of an $(L+1)$-point FFT is the same

as an (L+1)-point FHT, and that the IRS cross-correlation comprises a forward FFT followed by an inverse FFT both of length 4(L+1), then the 2L-point IRS cross-correlation will take approximately 8 times as long to execute as an L-point MLS cross-correlation by FHT. In a 386 PC based system this does not present a serious problem since a 2046-point IRS cross-correlation, coded in C language, can be performed in about 10 seconds. Although this is quick enough for on-site measurements, the cross-correlation would be faster if assembly level routines were used, or if FHT routines were developed for IRS.

Finally we should note that inverse repeat sequences are not the only signals that possess complete immunity to even-order nonlinearity whilst also displaying favourable 1st-order autocorrelation characteristics. Ternary sequences, *i.e.* periodic signals with three levels generated from a shift register using modulo-3 arithmetic [28], [29], possess both of these characteristics and in fact show a third-order distortion immunity advantage over both MLS and IRS due to their superior third-order autocorrelation characteristics. Nevertheless ternary sequences suffer from two disadvantages compared to IRS. First, three-level ternary sequences are more difficult to generate than binary IRS signals which only require a simple switch circuit for digital-to-analog conversion (although this hardly represents much of an obstacle given the wide availability of low-cost, high-performance multibit digital-to-analog converters). Second, cross-correlation routines for use with three-level ternary sequences cannot utilise the efficient FHT, because the FHT will only perform crosscorrelations for driving sequences with binary coefficients. More research is required upon the use of ternary and higher-order sequences in linear transfer function measurement.

7 CONCLUSIONS

A simulated comparison of PIE and MLS impulse measurement techniques has shown that, given optimal excitation amplitudes, MLS methods possess superior overall error immunity. For excitations of equal peak voltage and period L, MLS offers a 10 $\log_{10}(L+1)$ dB noise immunity advantage over PIE, but suffers a distortion immunity disadvantage when the test device bandwidth is significantly lower than half the system sampling frequency. Once optimal excitation amplitudes have been established, the exact overall MLS error immunity advantage depends upon the characteristics of the system under test, but will for all cases be between 0 dB and 10 $\log_{10}(L+1)$ dB.

An investigation into nonlinear error distribution in MLS-derived impulse measurements has confirmed that, in general, the error is evenly distributed across the period of the recovered impulse response. Even-order nonlinearity tends to result in less evenly spread error distributions compared to odd-order error distributions, while as the order of nonlinearity increases, the error distributions become smoother and more evenly spread. Memory in the nonlinearity also tends to smooth the even-order error distributions. Further simulations have shown that the amplitude distribution of the filtered MLS is not necessarily the major factor in determining the error distribution.

The even spread of error across the measurement period for both noise and nonlinearity has several important implications for MLS measurements. Firstly the tendency towards separation of linear and error components of the recovered impulse response can be used to monitor the relative error level in an MLS measurement and adjust excitation amplitude for optimal error immunity, a feature that is not available with PIE. Second, MLS noise and distortion immunity can be enhanced by truncating the recovered impulse response after the linear part of the impulse has decayed to zero. In fact maximum overall error immunity from a given MLS measurement system is obtained by choosing the longest period available and truncating the recovered impulse response as early as possible. Finally it is important to remember that the evenly spread MLS distortion error can also corrupt certain measurements such as cumulative spectral decay plots, although care taken in setting the stimulus amplitude should ensure that in most circumstances MLS offers superior performance compared to PIE.

The nonlinear impulse artifacts in MLS can be described in terms of the nonlinear kernels of the system under test and the higher-order autocorrelation functions of the unfiltered MLS signal. Inverse repeat sequences can be formed by inverting every other sample of an MLS, and they possess even-order autocorrelation functions equal to zero. This feature endows IRS measurements with complete immunity to even-order nonlinearity in the test device. Furthermore, for test devices where the bandwidth is significantly lower than the sampling frequency of the measurement system, IRS will also show some error immunity advantage over MLS for odd-order nonlinearity. An IRS shows no disadvantages compared to MLS other than a halving in measurable impulse length given a hardware memory limit, and an increase in cross-correlation time which is of small consequence for typical measurement periods.

8 ACKNOWLEDGEMENT

This work was supported by the Science and Engineering Research Council, UK. The authors would like to thank John Vanderkooy of the University of Waterloo for many fruitful discussions during a 4-month stay at the University of Essex, and also Richard Greenfield of Essex Electronic Consultants. They would also like to acknowledge the many helpful comments and suggestions made by the reviewers upon previous versions of the manuscript.

9 REFERENCES

[1] R.G.Greenfield and M.O.J.Hawksford, "Efficient Filter Design for Loudspeaker Equalisation," *J.Audio Eng.Soc.*, vol.39, pp.739-751 (1991 Oct.).

[2] C.Dunn and M.O.J.Hawksford, "Towards a Definitive Analysis of Audio System Errors," presented at the 91st Convention of the Audio Engineering Society, *J.Audio Eng.Soc. (Abstracts)*, vol.39, p.994 (1991 Dec.), preprint 3137.

[3] J.M.Berman and L.R.Fincham, "The Application of Digital Techniques to the Measurement of Loudspeakers," *J.Audio Eng.Soc.*, vol.25, pp.370-384 (1977 June).

[4] D.Rife and J.Vanderkooy, "Transfer-Function Measurement with Maximum-Length Sequences," *J.Audio Eng.Soc.*, vol.37, pp.419-444 (1989 June).

[5] J.Vanderkooy, "Another Approach to Time Delay Spectrometry," *J.Audio Eng.Soc.*, vol.34, pp.523-538 (1986 July/Aug.).

[6] H.Beiring and O.Z.Pederson, "Comments on "Another Approach to Time-Delay Spectrometry"," and author's reply, *J.Audio Eng.Soc. (Letters to the Editor)*, vol.35, pp.145-146 (1987 Mar.).

[7] R.Greiner, J.Wania and G.Noejovich, "A Digital Approach to Time-Delay Spectrometry," *J.Audio Eng.Soc. (Engineering Reports)*, vol.37, pp.593-602 (1989 July/Aug.).

[8] J.Atkinson, "Measuring with MELISSA," *Stereophile*, vol.13, no.2, pp.118-119 (1990 Feb.).

[9] M.Colloms, Loudspeaker Reviews, *Hi-Fi News and Record Review*, vol.35, no.12, pp.51-63 (1990 Dec.).

[10] K.R.Godfrey and W.Murgatroyd, "Input-transducer errors in binary crosscorrelation experiments," parts 1 and 2, *Proc. IEE*, vol. 112, pp. 565-573 (1965 Mar.), vol. 113, pp.185-189 (1966 Jan.).

[11] J.Vanderkooy, "Aspects of MLS Measuring Systems," presented at the 9third Convention of the Audio Engineering Society, (1992), preprint 3398.

[12] J.Borish and J.B.Angell, "An Efficient Algorithm for Measuring the Impulse Response Using Pseudorandom Noise," *J.Audio Eng.Soc.*, vol.31, pp.478-488 (1983 July/Aug.).

[13] J.Borish, "Self-Contained Crosscorrelation Program for Maximum-Length Sequences," *J.Audio Eng.Soc (Engineering Reports)*, vol.33, pp.888-891 (1985 Nov.).

[14] J.Borish, "An Efficient Algorithm for Generating Colored Noise Using a Pseudorandom Sequence," *J.Audio Eng.Soc.*, vol.33, pp.141-144 (1985 Mar.).

[15] C.Swerup, "On the Choice of Noise for the Analysis of the Peripheral Auditory System," *Biological Cybernetics*, vol.29, pp.97-104 (1978).

[16] H.Alrutz and M.R.Schroeder, "A Fast Hadamard Transform Method for the Evaluation of Measurements Using Pseudorandom Test Signals," *Proc. 11th Int. Conf. on Acoust.*, pp. 235-238 (Paris, 1983).

[17] C.Dunn and M.Hawksford, "Distortion Immunity of MLS-derived Impulse Response Measurements," *Proc.IOA*, vol.13, part 7, pp.191-206 (1991).

[18] D.R.Rife, "Modulation Transfer Function Measurement with Maximum Length Sequences," *J.Audio Eng.Soc.*, Vol.40, No.10, pp.779-789 (1992 Oct.).

[19] M.R.Schroeder, "Integrated-Impulse Method for Measuring Sound Decay Without Using Impulses," *J.Acoust.Soc.Am.*, vol.66, pp.497-500 (1979 Aug.).

[20] S.W.Golomb, "Shift Register Sequences," Holden-Day, San Francisco (1967).

[21] J.D.Bunton and R.H.Small, "Cumulative Spectra, Tone Bursts and Apodization," *J.Audio Eng.Soc.*, vol.30, pp.386-395, (1982 June).

[22] S.P.Lipshitz, T.C.Scott and J.Vanderkooy, "Increasing the Audio Measurement Capability of FFT Analyzers by Microcomputer Postprocessing," *J. Audio Eng. Soc.,* vol.33, pp.626-648 (1985 Sept.).

[23] S.H.Tsao, "Generation of Delayed Replicas of Maximal-Length Sequences," *Proc.IEE*, vol.111, pp.1803-1806 (1964 Nov.).

[24] H.R.Simpson, "Statistical Properties of a Class of Pseudorandom Sequences," *Proc.IEE*, vol.113, pp. 2075-2080 (1966 Dec.).

[25] W.H.Press et al., *Numerical Recipes in C: The Art of Scientific Programming* (Cambridge University Press, Cambridge, UK, 1988).

[26] N.Ream, "Nonlinear Identification using Inverse Repeat Sequences," *Proc.IEE*, vol.117, pp.213 - 218 (1970 Jan.).

[27] P.A.N.Briggs and K.R.Godfrey, "Pseudorandom Signals for the Dynamic Analysis of Multivariable Systems," *Proc.IEE*, vol.113, pp.1259-1267 (1966 July).

[28] E.P.Gyftopoulos and R.J.Hooper, "Signals for Transfer-Function Measurement in Nonlinear Systems," *Proc. Noise Analysis in Nuclear Systems,* USAEC Div. of Tech. Inf., Symposium Series 4 (TID-7679), pp.335-345 (1964).

[29] E.P.Gyftopoulos and R.J.Hooper, "On the Measurement of Characteristic Kernels of a Class of Nonlinear Systems," *Neuron Noise, Waves and Pulse Propagation,* USAEC Div.of Tech.Inf., Report 660206, pp.343-356 (1967).